Master Thesis
TVVR 21/5016

Coastal Response to Sea Level Rise in Ystad Municipality

Development, comparison and application of Bruun Rule-based methods

Sara Engström
Elin Olsson

Division of Water Resources Engineering
Department of Building and Environmental Technology
Lund University

Coastal Response to Sea Level Rise in Ystad Municipality

Development, comparison and application of Bruun Rule-based methods

By:
Sara Engström
Elin Olsson

Master Thesis

Division of Water Resources Engineering
Department of Building & Environmental Technology
Lund University
Box 118
221 00 Lund, Sweden

Water Resources Engineering
TVVR-21/5016
ISSN 1101-9824

Lund 2021
www.tvrl.lth.se

Master Thesis
Division of Water Resources Engineering
Department of Building & Environmental Technology
Lund University

Swedish title:	Kustlinjeförändringar till följd av stigande havsnivåer i Ystad kommun
English title:	Coastal Response to Sea Level Rise in Ystad Municipality
Author(s):	Sara Engström Elin Olsson
Supervisor:	Caroline Hallin, Anna Adell, Sebastian Bokhari Irminger
Examiner:	Magnus Larson
Language:	English
Year:	2021
Keywords:	Coastal erosion; Bruun Rule; Sea level rise; Coastal management; beach morphology; coastal processes

Acknowledgements

We want to thank our supervisors, Caroline, Anna and Sebastian, for inspiration, encouragement and support. Your knowledge and enthusiasm have helped us tremendously in our first contact with the research area. Thank you also for believing in our ideas and helping us pursue them.

We would also like to thank Mona Skoog for providing information of Ystad, Björn and Hans for their input on our work, Lars-Johan and Britta who gave us a valuable introduction to literature searching, Magnus who magically had 99 % of the literature we could not access and Martin for helping us navigate the Monte Carlo simulation.

Lastly, but not least, we would like to thank our friends and family who supported us when we faced difficulties and listened with patience when we for the 100^{th} time went on about the faith of small sand grains.

Abstract

The globally accelerating sea-level rise poses a problem in coastal areas through, e.g., the erosion of sandy beaches. Due to this, buildings, infrastructure, and other values can be lost, making the future shoreline position important to project in coastal management. One location with historical erosion problems is Ystad municipality in southern Sweden, where the erosive problems are probable to worsen with accelerated SLR. To quantify these problems, calculation methods for projecting the future shoreline change are of high importance, and a commonly used method is the Bruun Rule. The Bruun Rule estimates the shoreline recession due to changes in forcing conditions during sea-level rise. However, the method is coupled with restrictive assumptions and has been widely criticised. Due to this, several modifications of the Bruun Rule exist in the literature, but no other has seen global application in coastal management. In this thesis, Bruun Rule-based methods are identified, developed, and then qualitatively compared to the Bruun Rule to evaluate the effects of alternative calculation methods in Ystad municipality.

First, to detect coastal processes affecting the studied coastline and calculation methods corresponding well to the conditions in Ystad municipality, a literature study was performed. To compare the methods, four beach profiles in areas with different states of historical erosion were chosen for application, and data was compiled. Finally, the future shoreline changes for the beach profiles in 2150 were estimated by each method, and the results qualitatively compared. In addition, a simplified Monte Carlo analysis was performed to visualise the data uncertainties.

What could be concluded from the comparison was that including the effect of the background erosion/accretion, assumed to be constant over the studied period, in some profiles overshadowed the effect from the SLR-induced erosion by the Bruun Rule. Modifying the Bruun Rule to include the dune system, assumed not to migrate inland, gave lower recession with the given dune dimensions, but still in the same order of magnitude as the Bruun Rule. Furthermore, the low availability of sand along the coastline of Ystad municipality resulted in the conclusion that the Bruun Rule is not applicable on the majority of the coastline. The results from the Monte Carlo simulation

showed that the large uncertainties in data resulted in probability intervals of up to 90 m for the projected shoreline change using the Bruun Rule.

Thus, when calculating shoreline change in Ystad municipality, methods applicable on non-sandy beaches are needed, in addition to the Bruun Rule, better access to detailed data is essential, and the underlying erosion is an important factor to consider for coastal management purposes.

Sammanfattning

Den globalt accelererande havsnivåhöjningen utgör ett hot mot kustnära områden genom bl.a. erosion av stränder. På grund av detta kan byggnader, infrastruktur och andra värden förloras, således är strandlinjens framtida position en viktig komponent att approximera inom kustförvaltning. Ett område med historiska erosionsproblem är Ystad kommun i södra Sverige, där problemen även förväntas förvärras med den accelererande havsnivåhöjningen. För att kunna kvantifiera problemen är det viktigt med beräkningsmetoder som kan uppskatta den framtida strandlinjeförändringen, och vanligen används metoden Bruuns lag. Bruuns lag estimerar strandlinjens tillbakadragning till följd av en förändrad jämvikt mellan krafterna i kustzonen, som orsakas av havsnivåhöjningen. Dock är modellen förknippad med restriktiva antaganden och har därmed blivit vida kritiserad. Därför finns det idag flera utvecklingar av Bruuns lag i litteraturen, men ingen annan beräkningsmetod har inkorporerats i praxisen för kustförvaltning på en global skala. I detta exjobb identifieras och utvecklas Bruuns lag-baserade modeller och jämförs sedan kvalitativt mot Bruuns lag för att utvärdera effekten av alternativa beräkningsmetoder i Ystad kommun.

För att kartlägga kustprocesser som påverkar den studerade kuststräckan, och beräkningsmetoder som korresponderar med förhållandena i Ystad kommun, utfördes en litteraturstudie. För att kunna jämföra metoderna valdes fyra strandprofiler ut i områden med olika erosionshistorik för applicering, och därefter sammanställdes data. Till slut estimerades den framtida strandlinjeförändringen för 2150 för de fyra profilerna med hjälp av varje metod, och resultaten jämfördes därefter kvalitativt. Dessutom utfördes en simplifierad Monte Carlo analys för att visualisera osäkerheter i data.

Det som kunde konstateras från jämförelsen var att inkluderandet av effekten från bakgrundserosionen/-ackumulationen, antaget att den fortsatte konstant över hela den studerade tidsperioden, överskuggade effekten från havsnivåhöjningen från Bruuns lag i vissa profiler. Att modifiera Bruuns lag till att ta hänsyn till dynsystemet, antaget att det inte förflyttas inåt land, gav en kortare tillbakadragning av strandlinjen än Bruuns lag med de givna dyndimensionerna, men fortfarande i samma storleksordning. Dessutom resulterade den låga sandtillgången längs Ystad kommuns kuststräcka i slutsatsen att Bruuns lag inte är applicerbar på majoriteten av kusten.

Resultaten från Monte Carlo simuleringen visade att de stora osäkerheterna i data gav sannolikhetsintervall på uppemot 90 m för den projicerade strandlinjeförändringen beräknad med Bruuns lag.

Därmed är behovet av metoder för stränder utan tillräckligt med sand, utöver Bruuns lag, stort för att kunna beräkna strandlinjeförflyttningen i Ystad kommun, bättre tillgång till detaljerade data är nödvändig, och den underliggande erosionen är en viktig faktor att inkludera i kustförvaltningssyfte.

Table of contents

1 Introduction

Coastal erosion is likely to increase in the future due to an accelerated sea-level rise (SLR) caused by global warming. The shoreline recession threatens residences and infrastructure in the coastal area as well as coastal ecosystem services (IPCC, 2019). Thus, the recession from SLR is an important aspect to include in coastal management, e.g., in flood and erosion risk assessment and planning processes. One location where shoreline recession is a problem already today is Ystad municipality. The coastline is experiencing some of the worst erosion in Sweden; properties have been lost, and sections of the national highway along the coast are at risk (Borell Lövstedt and Persson, 2015). The problems are expected to aggravate in the future with rising sea levels (SMHI, 2018) and reliable methods to predict the future shoreline position are needed.

When addressing the future recession from SLR in coastal management, a common method is the Bruun Rule developed by Bruun (1962), which only accounts for SLR as the process to drive the erosion. However, the Bruun Rule has been criticised both for its restrictive assumptions and the usage in coastal management to project the future recession (Cooper and Pilkey, 2004; Davidson-Arnott, 2005; Wolinsky and Brad Murray, 2009; Rosati, Dean and Walton, 2013; Dean and Houston, 2016; Cooper *et al.*, 2020). The restrictive assumptions of the Bruun Rule fit only a minority of the natural beaches, but this is often overlooked in application (Cooper and Pilkey, 2004; Cooper *et al.*, 2020). For example, the method is limited to well-sorted sandy beaches and does not consider the effect of the dune system or other morphological features present (Davidson-Arnott, 2005). In addition, the total shoreline recession in the future will not only be caused by SLR, but other factors will have a large impact, depending on location (Dean and Houston, 2016). Using solely the Bruun Rule in coastal management to predict the shoreline recession poses a problem with potential negative societal, ecological, and economic consequences. To widen the applicability by eliminating some of the restrictive assumptions and also accounting for other factors, many developments of the Bruun Rule have been presented over the years (e.g., Dean and Maurmeyer, 1983; Rosati, Dean and Walton, 2013; Young *et al.*, 2013; Dean and Houston,

2016). However, they are not applied as extensively in coastal management as the Bruun Rule, and general recommendations and incorporation into the common practice are needed.

1.1 Objectives and Research Questions

The intention of this thesis is to contribute to the development and improvement of calculation methods in the coastal management field. The main objectives are to (1) identify and develop Bruun Rule-based methods for future shoreline recession and (2) qualitatively compare the recession calculated with the original Bruun Rule and its developments. This thesis aims to answer the following questions:

- How applicable is the Bruun Rule within the study area?
    - How do the results differ depending on the methods used to estimate shoreline change?
    - What effect on the result does it have to include the dune system in the model?
- How large is the contribution from SLR-induced recession compared to the total shoreline change?

This study is limited to Ystad municipality and Bruun Rule-based methods. Projections are made for the year 2150 due to the long-term planning perspective and the technical lifetime of, e.g., infrastructure projects.

1.2 Methodology of the Study

A literature study was conducted with the aim to compile relevant information regarding coastal processes within the study area and identify methods to estimate shoreline recession suitable for application and comparison in the studied area. During the literature study, the data needed for the application of the models were identified.

The data needed were compiled from existing sources; no field measurements were conducted. For example, SLR projections were collected from Intergovernmental Panel on Climate Change (IPCC), data containing

information of the geology were provided by the Geological Survey of Sweden (SGU), national elevation data were obtained from Lantmäteriet, wave records were extracted from a wave hindcast model by Adell *et al.* (2021) and grain size measurements from another master thesis by Berin and Löwdin (2021) conducted at the time of writing. ArcGIS was used to visualise and extract data from, e.g., the national elevation model and Excel was used to process the data into the required input format.

Based on the literature study and available data, four beach transects within different sections of the studied area were selected for model application. The recession calculations were then performed on each transect using Python-scripts and Excel sheets, and the results were compared.

A sensitivity analysis was conducted on the Bruun Rule to identify the parameters most sensitive to measuring errors. A Monte Carlo simulation was conducted to investigate the effects of data uncertainties in the Bruun Rule and Dean Houston-model.

1.3 Structure of Thesis

Chapter 2 – Theory gives relevant background theory for this study. Processes related to coastal recession in Ystad municipality are explained, and previous research on the coastal response to SLR is presented. In addition, the Bruun Rule with its assumptions and extensions are introduced.

Chapter 3 – Case Study Site introduces the study area and lists some erosion related problems and protective measures.

Chapter 4 – Methodology and Data presents the method used to select beach profiles for model application, and the different equations and models applied, followed by a summary of data sources used to estimate the input parameters to the calculations. The chapter also describes the sensitivity analysis and Monte Carlo simulation performed.

Chapter 5 – Results and Discussion presents, compares, and discusses the results from the calculations performed.

Chapter 6 – Conclusions and Recommendations summarises the conclusions of this study and presents some recommendations for future studies and the use of the Bruun Rule in coastal management.

2 Theory

The first three sections of this chapter present an overview of the morphological features and coastal processes of importance in this study, with main focus on sandy beaches. The final section summarises previous research of coastal response to SLR and presents the Bruun Rule with its assumptions and a number of developments.

2.1 Hydrodynamic Forcing

Hydrodynamic forcing includes wave action and nearshore currents acting in the coastal area and influencing the beach morphology.

The primary energy input to the coastal zone is wind-generated waves, which compose an important force governing the coastal morphology (US Army Corps of Engineers, 1984; Davidson-Arnott, 2010). The wind-generated waves, induced by the transfer of energy from the wind to the water surface, move in an oscillatory pattern in the direction of the generating wind. When the waves reach shallow water, the wave energy is dissipated, primarily during breaking but also by bottom friction and run-up on the beach (Davidson-Arnott, 2010).

The wind-generated waves are irregular and random in their form and direction; thus, difficult to describe mathematically. A fundamental theoretical description of the wind-generated waves in deep water is by a series of different symmetrical sinusoidal waves. Figure 2.1 presents a simplified representation of a single sinusoidal wave. The water particles under a sinusoidal wave move in orbital patterns, which decrease with depth, being negligible at the bottom (Davidson-Arnott, 2010). As the waves move into the shallow water by the coast, the interaction with the bottom causes a reshaping of the waves into an asymmetrical form, with a net onshore movement (Bruun, 1988). The motion pattern of the water particles then gradually changes from orbital into being more elliptical with shallower water, with only a horizontal movement along the bottom (Figure 2.2) (Davidson-Arnott, 2010). Different from the sinusoidal wave is the solitary wave, where the wave tends towards moving faster, only forward and above the mean water level in a semi-elliptical motion. The elliptical movements of the water particle in shallow water are a combination

of sinusoidal and solitary waves, with a general tendency towards more solitary-like waves (Fenneman, 1902).

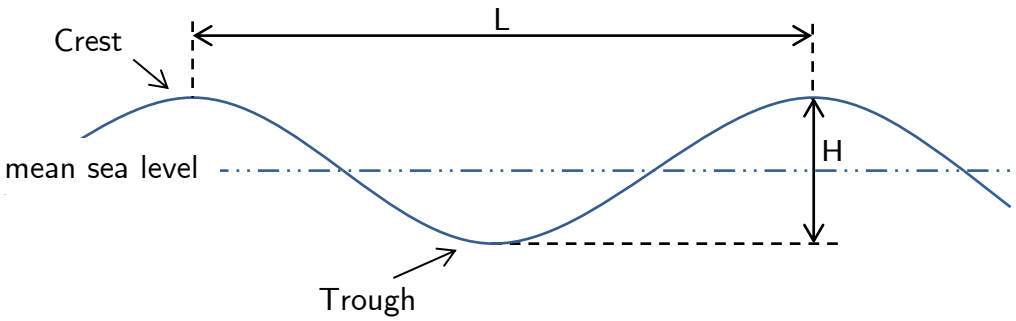

Figure 2.1: Schematic picture of a simple sinusoidal wave. Modified from US Army Corps of Engineers (1984).

Waves can be characterised by wavelength *(L)*, wave height *(H)* and wave period *(T)* (Figure 2.1). The wave length is the distance between two adjacent wave crests, the wave height is the vertical distance between a wave crest and the preceding trough, and the wave period is the time for two succeeding crests to pass a fixed point (US Army Corps of Engineers, 1984). The *significant wave height* (H_S) is a parameter that represents the wide range of wave heights in wave measurements and is commonly used in engineering applications. The significant wave height is defined as the average height of the one third-highest waves of the record (US Army Corps of Engineers, 1984).

When waves approach the shore, a temporary increase in the water level (setup) is created due to the net onshore movement of water. The difference in water level generates nearshore currents, a flow of water from areas with higher water levels to lower levels. Nearshore currents can be either cross-shore directed, such as undertow or rip cell circulations (Leatherman, Zhang and Douglas, 2000) or longshore directed (Davidson-Arnott, 2010). If the waves approach the shore perpendicular, a seaward directed return flow is generated to balance the setup. The return flow can be either in the form of an undertow, a two-dimensional flow along the bottom or a three-dimensional rip cell circulation,

where the return flow is concentrated in narrow channels (Davidson-Arnott, 2010). If the waves approach the shore with an oblique angle, a part of the wave's longshore motion component will be translated into a current directed parallel to the shore, termed longshore current. The direction and magnitude of longshore currents are sensitive to the angle of wave approach and will change with changed wave conditions (US Army Corps of Engineers, 1984).

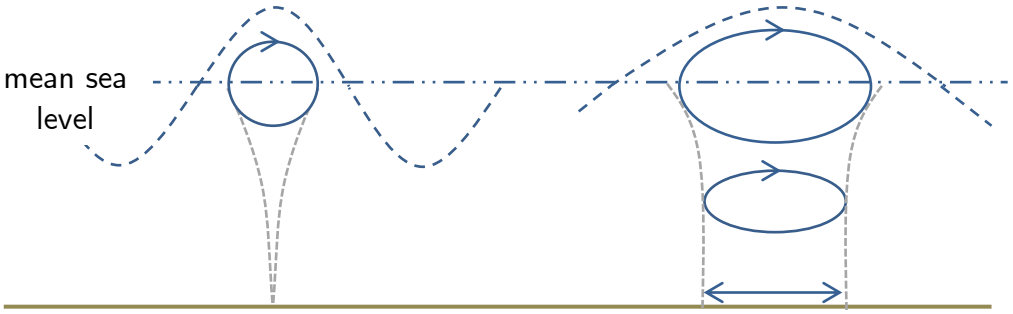

Figure 2.2: Wave motion patterns of a water particle in deep water (left) and shallow water (right). Modified from US Army Corps of Engineers (1984).

2.2 Morphology of the Coastal Zone

An understanding of the coastal morphology and the forcing conditions affecting it is fundamental when modelling shoreline response since the beach area is dynamic and will change with varying conditions. The longshore and cross-shore perspectives in morphology are often looked at separately, where the Bruun Rule estimates changes in the cross-shore beach profile.

The coastal zone consists of different cross-shore sections created by the present forcing conditions and material characteristics, presented in Figure 2.3. The beach, or shore, is the zone between the mean sea level and the landward limit of wave action, usually extending to the dune foot. One or several horisontal plateaus, so-called berms, with vertical cuts at the end, are morphological features at the shore. The shore is backed by a dune system, created by depositions of sand transported from the beach by wind action (Davidson-Arnott, 2010). Seaward of the shore, the nearshore zone extends out to a depth where wave-induced currents no longer affect the bathymetry, termed the *depth of closure* (DoC) (Hallermeier, 1978). The landward part of the nearshore zone is termed the surf zone, where the waves break.

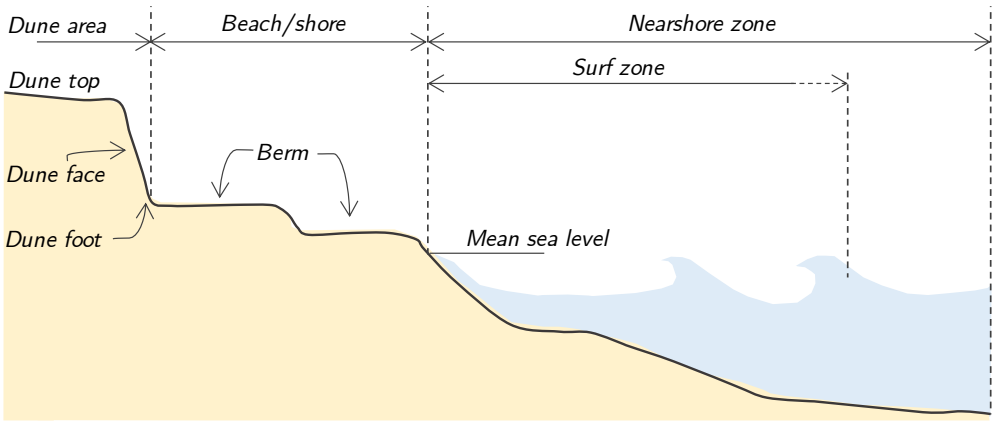

Figure 2.3: Schematic picture of a beach profile's different zones. Modified from US Army Corps of Engineers (1984)

The shore and nearshore section together form the *active profile*, which is highly influenced by waves and currents. A major part of the transport of

sediment takes place within this profile, and the main profile changes occur within the surf zone (US Army Corps of Engineers, 1984; Davidson-Arnott, 2010).

2.2.1 The Equilibrium Profile

The equilibrium profile is a central concept in coastal response analysis (Larson, Kraus and Wise, 1998) and is considered a powerful tool by engineers (Dean, Kriebel and Walton, 1995). In nature, the active profile is dynamic, and the shape is continuously adapting to changing wave conditions and water level, where the upper part changes the fastest (Stive and de Vriend, 1995). Still, averaged over a long period of time, the active profile can reach an equilibrium state, consistent in shape (Bruun, 1954; Dean and Dalrymple, 2004). Further, it requires that the forces acting on the beach are in long term balance with no net gain or loss of sediment over the profile (Dean, Kriebel and Walton, 1995; Dean and Dalrymple, 2004). The equilibrium profile is governed by the grain size, amount of sediment in the system and different forcing conditions (Rosati, Dean and Walton, 2013). If the beach profile contains rigid geological structures or elements of coarser sediment, the profile shape will be affected, and a dynamic equilibrium shape cannot be formed (Gallop et al., 2020). In calculations, the seaward limit of the equilibrium beach profile is commonly defined as the DoC (Bruun, 1962; Pilkey *et al.*, 1993; Dean and Houston, 2016, etc.), and the landward limit has different definitions, e.g., the berm, wave runup limit or the dune foot (Dean, Kriebel and Walton, 1995).

The subaqueous part of the equilibrium profile has been highly researched, described for the first time by (Bruun, 1954), with several equations with even more modifications (Dean, 1977; Boon and Green, 1989; Kriebel, Kraus and Larson, 1991; Larson, 1991; Bodge, 1992; Komar and McDougal, 1994; Türker and Kabdaşli, 2004, 2006; Holman *et al.*, 2014). However, the most common subaqueous profile equation is the Dean profile, presented later in section 4.2 . The shape of the subaqueous profile is generally concave, and its dimensions depend on wave conditions and sediment type. Steeper waves and finer sediment both create a milder slope, while a steeper slope is associated with coarser sediment (Dean, 1991).

2.2.2 The Beach Sediment

The beach sediment, together with the forcing conditions, has a large effect on the beach morphology (Preoteasa and Vespremeanu-stroe, 2010). Worldwide, beaches are depositions of loose sediment of various sizes. However, most of the world's beaches consist of sand (Bird, 2000). Coastlines with a high amount of fine sediment (i.e., clay and silt) have a different response to the forcing conditions due to the cohesive forces between the grains. Therefore, these coastlines are conventionally excluded from the definition of beaches and instead referred to as muddy coast (Bird, 2000; Davidson-Arnott, 2010). Also, moraine coastlines have a different response to forcing conditions due to the portion of clay and larger grains in the sediment (Nyberg et al., 2020).

Sediment types are typically classified based on the median grain size (Table 2.1), where sand lies in the range 0.06 – 2 mm. When measuring the beach sediment, the reference point is usually the Bascom point because it shows little variation over time and can be correlated to the slope of the profile (Bascom, 1951). The Bascom point lies in the mid-tide elevation, defined as the point *"between the previous high tide and the succeeding low tide"* (Mcfall, 2019). The grain size distribution is another parameter used to classify the beach sediment; sediment can be well sorted, containing only a small range of grain sizes, or poorly sorted (Bird, 2000).

Table 2.1: Standard sizes of sediments based on diameter (d) in mm.

Type		d (mm)
Clay		< 0.002
Silt		$0.002 - 0.06$
Sand	Fine	$0.06 - 0.2$
	Medium	$0.2 - 0.6$
	Coarse	$0.6 - 2$
Gravel		$2 - 60$
Cobbles		> 60

The grain size across the profile is often assumed uniform when modelling the morphological evolution. However, Koktas (2017) showed the importance of accounting for the variation in grain size distribution across the profile. The variation originates from a sorting process depending both on the variation in forcing conditions across the beach profile and the grains' threshold of motion, which increases rapidly with grain size and density (Davidson-Arnott, 2010). The sorting process leads to different grain sizes tend to accumulate in different zones across the profile (Figure 2.4). In the subaqueous part of the coastal zone, the movement of one specific grain with a certain threshold of motion and specific gravity depends on the balance between forces induced by the asymmetrical waves and gravity, reaching for an equilibrium state (Bruun, 1988). The dune system often contains finer sediment than in the Bascom point since the wind action mobilises finer grains (Preoteasa and Vespremeanu-stroe, 2010). Coarser grains are typically found in the zones where the turbulence is high due to wave action (plunge point), and finer sediments are moved offshore (Dean, 1977)

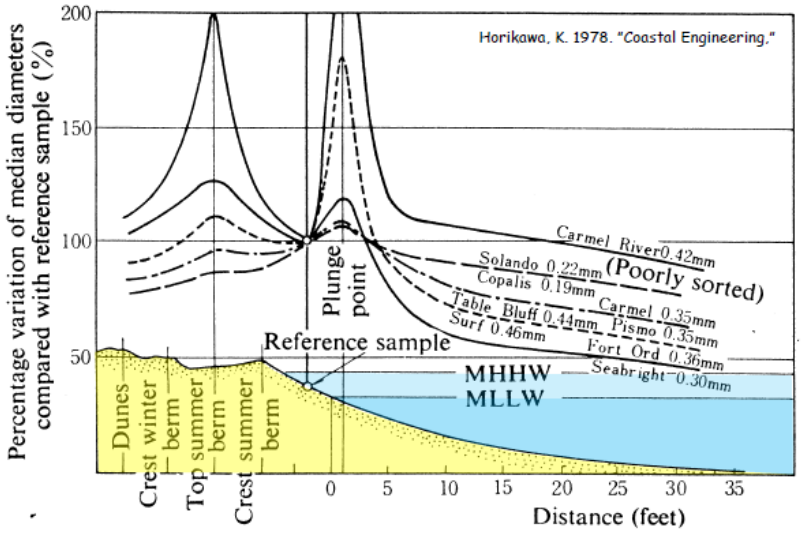

Figure 2.4: Variation in grain sizes across different beach profiles compared to the Bascom reference point ("reference sample" in the figure). *Source: (Bascom, 1951).*

2.3 Sediment Transport Processes

Sediment transport is the movement and relocation of beach sediment in the coastal zone, induced by shear stress exerted by the hydrodynamic forcing described in Section 2.1 and wind forcing. It also depends on the beach sediment's characteristics. The transport co-occurs in the cross- and longshore direction but is often described separately due to the different time scales. The sediment transport in the coastal area can cause beach erosion or accretion and affects the beach profile's shape (Davidson-Arnott, 2010).

To investigate the erosion, or accretion, of a delimited section of the coast (control volume) and specific time frame, the *sediment budget* concept is commonly used, illustrated in Figure 2.5. The sediment budget is a mass balance of the transport into and out from the control volume and contributions of other anthropogenic additions or removals of sand. When there is no net change in volume, the sediment budget is balanced, and the delimited coastal section is stable. The balance of the sediment budget depends on different processes, for example, the longshore and cross-shore sediment transport in and out of the control volume and anthropogenic sinks and sources (Rosati, 2005). The processes affecting the sediment budget are described in more detail in sections 2.3.1 – 0. By quantifying all different sediment volumes entering and exiting the control volume, the sediment budget can be formulated, and the resulting deficit or excess of sediment volume be determined according to Equation (2.1):

$$\frac{dV}{dt} = \sum Q_{in} - \sum Q_{out} \tag{2.1}$$

where Q_{in} and Q_{out} are the incoming and outgoing sediment flow to the control volume, respectively. A balanced cell will not experience any erosion or accretion (Rosati, 2005).

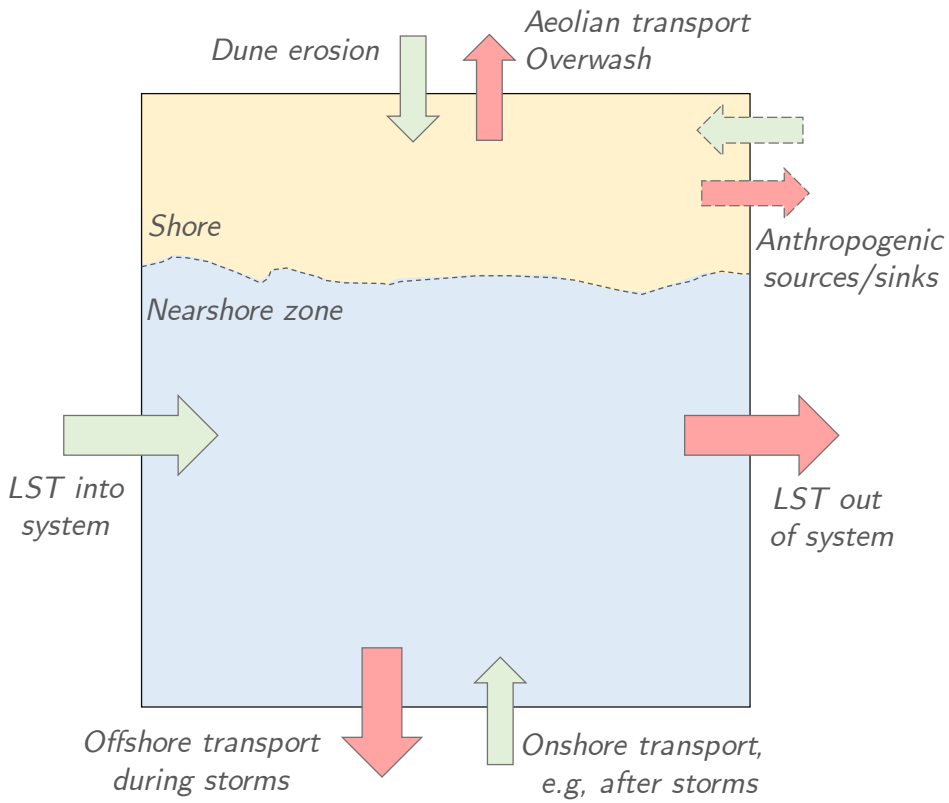

Figure 2.5: Plan view of the sediment budget concept for a section of the coast. The green arrows represent volumes entering the system (Q_{in}), while the red represent volumes exiting the system (Q_{out}).

2.3.1 Longshore Sediment Transport

Longshore sediment transport (LST) is highly important in most coastal areas since it is responsible for a large part of the shoreline's long-term changes (Davidson-Arnott, 2010) and refers to the transport running parallel to the beach. The sediment particles are suspended by the breaking waves and transported by the wave-induced longshore current. In general, tidal currents may also contribute but are not discussed here as they are not relevant for the conditions in Ystad.

The transport rate in the longshore direction depends on incoming wave properties (wave energy, angle of approach and duration); thus, the transport varies over time (US Army Corps of Engineers, 1984). The most sensitive parameter of longshore sediment transport is the inclination angle of the incoming waves to the coast (Tegenfeldt and Johansson, 2020), and since the shoreline is not entirely rectilinear, the transport rate can vary along the shore. These gradients in the LST rate create a sediment budget imbalance, leading to erosion or accretion in different places. When investigating coastal evolution and erosion in a long-term context, the average annual net transport rate is highly important to address (Davidson-Arnott, 2010).

Estimating the LST gradient *(dQ/dy)* can be done with several methods. One method is to perform a shore- or vegetation line analysis using orthophotos from different periods. The change in meters per year (m/yr) is converted to cubic meters per meter beach per year ($m^3/m/yr$) by multiplication with the height of the active profile (Fredriksson *et al.*, 2017). This method risks overestimating the LST gradient as some of the sediment loss identified might be due to cross-shore transport during storms, and this sediment might still be within the control volume. It may also underestimate the LST gradient since it does not capture the changes in the subaqueous part of the profile. In addition, as orthophotos present an instantaneous view, the shoreline position is sensitive to momentary deviations caused by water level conditions. Another method is by calculating the volume difference between bathymetry measurements performed at different times for a control volume (US Army Corps of Engineers, 1984). The LST-gradient is then calculated using Equation (2.2), where ΔV is the volume change, L the length of the control volume, and Δt the time between measurements (Figure 2.6). This method accounts for the whole sediment budget of the transect, compared to the vegetation line analysis. However, also this method risks overestimating the LST due to cross-shore sediment loss.

$$\frac{dQ}{dy} = \frac{\Delta V}{L \cdot \Delta t} \tag{2.2}$$

A third method is to use sand traps on the bottom (Kraus and Dean, 1987). Finally, another way of estimating the LST gradient is to use a LST model, such as the CERC-formula, where the LST is calculated based on wave properties and incoming wave angle (Van Rijn, 2002) and over a stretch calculate $Q_{in} - Q_{out}$.

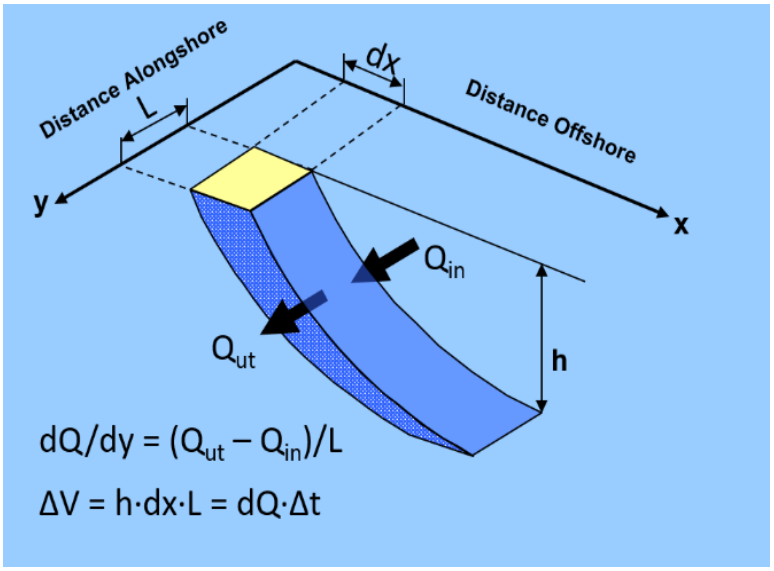

Figure 2.6: Schematic figure of how the LST-gradient can be determined from volume measurements. (Source: Hanson, H., 2021. Personal communication)

2.3.2 Cross-shore Sediment Transport

The cross-shore sediment transport is directed perpendicular to the shoreline and consists of many different forces acting both on- and offshore. Waves just before breaking typically exert a net onshore force, the wind can affect the dry beach in both directions, whereas gravity and undertow act in the offshore direction. If the forcing conditions are stable, an equilibrium is eventually reached between the on- and offshore forces, including gravity (Dean, 1987), only for the net transport to start again when conditions change (Dean, Kriebel and Walton, 1995). A phenomenon due to the on- and offshore forces is bar formations that form where onshore- and offshore forces meet (Davidson-

Arnott, 2012). In profiles where bars are present, the wave breaking is often concentrated over the bar, thus migrating the bar onshore (Holman *et al.*, 2014).

On most sandy beaches, the transport is directed offshore during stormy conditions when higher waves erode the upper beach profile and transport the sediment out to the lower beach profile. The transport is directed onshore during calmer conditions, returning the previously eroded sediment to the beach. On a decennial to centennial time scale, with no long-term SLR, the cross-shore transport tends to an equilibrium and might have a negligible effect on the change in coastline position (Davidson-Arnott, 2010). However, during extreme storms, the sediment might be transported and deposited outside the active profile, disappearing from the dynamic nearshore system. Storms can also cause severe erosion in the dune foot due to high energetic waves. The system may not always have the ability to recover; thus, the long-term coastal evolution is affected.

In the light of ongoing and future accelerating SLR, offshore losses of sediments are expected to be more dominant, as further discussed in section 2.4.

2.3.3 Dune Erosion and Build-up

Dunes are subaerial and can thus be affected by aeolian transport, i.e. wind transport, but they are usually still close enough to the shoreline to also be affected by the wave action during storm conditions (Davidson-Arnott, 2010). In aeolian transport, finer sediment is mobilised at lower wind speed than coarser grains (Short and Hesp, 1982). Another important factor in the dune erosion and build-up is the vegetation, usually present on the dunes, which affects the stability of the sand. The vegetation diminishes the wave erosion and increases the dune build-up due to aeolian transport (Lindell, Fredriksson and Hanson, 2017), where the vegetation decreases the wind shear stress, allowing for grains to deposit (Hallin, 2019). Another way the dune morphology is affected is by aeolian sand transport inland from the dunes, thus being a loss in the system (Lindell, Fredriksson and Hanson, 2017). Erosion of dunes due to wave action during a storm also depends on the runup height, duration of the surge and dune foot elevation (Larson, Erikson and Hanson, 2004).

Dunes of eroding beaches can either migrate inland, conserving its volume or even increase in volume or, if the erosion is significant and the over-wash prominent, the dune will be flattened and move inland (Hallin, 2019). Storms can cause erosion of the vegetated foredune, enabling aeolian transport to move sediment to the landward slope with less wind action. This, together with the erosion in the dune base, induces the landward migration of the dune. (Davidson-Arnott, 2005).

2.3.4 Beach Nourishment

Beach nourishment is a widely used coastal protection where sand is collected from, e.g., deep water and transported to erosive areas to preserve the beaches. The added sand is then eroded instead of the original shoreline, and the damages are reduced. The sand is usually placed either on the beach or the nearshore bottom (U.S. Army Corp of Engineers, 1995). The sand is then naturally spread across the profile, generally within the time of one year, and on a longer time scale spread along the shoreline (Karasu *et al.*, 2008). The cross-shore redistribution is sometimes considered as being uniform across the profile in modelling (Dean and Houston, 2016). However, in reality, the difference between the natural grain size and nourishment grain size has an impact on the slope of the profile and thus also the shoreline position (Dean, 1983).

The long term spread of a beach nourishment along the shore usually forms a bell shape that flattens gradually over time (Pelnard-Considere, 1956), seen in Figure 2.7. This spread is due to the perturbation of the initial shoreline orientation (Dean, 2002) and the refraction and diffraction of waves due to this (Larson, Hanson and Kraus, 1987), striving towards straight, parallel contours (Dean, 1983). This longshore spread is thus not the net longshore transport but the straightening out of the perturbation in morphology. The longshore spread can be simplified to the diffusion equation (Equation (2.3)), which can be solved for different conditions (Pelnard-Considere, 1956; Dean, 1983, 2002; Larson, Hanson and Kraus, 1987; Larson and Kraus, 1991).

$$\frac{\partial y}{\partial t} = \varepsilon \frac{\partial^2 y}{\partial x^2} \tag{2.3}$$

where x and y are the cross-shore and longshore distances, respectively, and the diffusivity, ε in m^2/s, describes the rate at which the sand spreads. The diffusivity depends strongly on the breaking wave height (Dean, 2002) and the angle of the incoming waves (Falqués, 2003). The diffusivity is also used when examining the beach response to cross-shore stretching barriers, such as groynes (Pelnard-Considere, 1956; Dean, 2002).

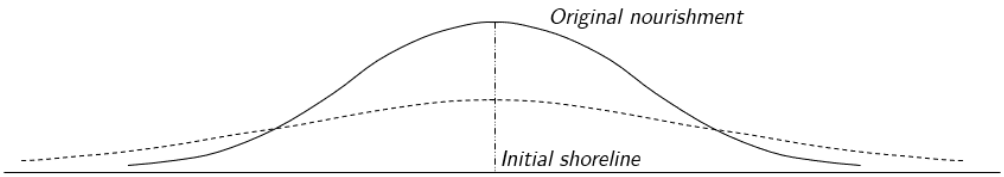

Figure 2.7: Plan view of the evolution of a beach nourishment over time. The rectilinear line at the bottom being the initial shoreline, the continuous line the initial beach nourishment and the middle, dashed line being the nourishment after some time. Modified from Pelnard-Considère (1956).

The assumptions made in plan view shoreline modelling are that the cross-shore profile is constant, the sediment is not transported across the DoC, and the LST depends on the incoming wave direction, which is assumed to be relatively close to the initial shoreline (Pelnard-Considere, 1956; Larson and Kraus, 1991).

2.4 Sea Level Rise

A rise in the mean sea level can significantly influence the processes governing the coastal morphology (Davidson-Arnott, 2010) and allow waves to reach areas previously unaffected by the hydrodynamic forcing conditions (Leatherman, Zhang and Douglas, 2000). The mean sea level has a natural fluctuation due to tides and meteorological processes. However, it has been shown that there is a long-term rise in sea level globally (Davidson-Arnott, 2010; IPCC, 2019). The rise in global mean sea level is produced by melting glacial ice sheets and the oceans' thermal expansion caused by the increase in the global temperature. With continued emissions and increasing global temperature in the future, the SLR will accelerate (IPCC, 2019). Even if the global warming is reduced, the processes inducing SLR have a slow response to the driving force, meaning that the sea level will continue to rise (SMHI, 2020b).

Predictions of the future global SLR have been presented by IPCC (2019). The predictions extend until 2300, however, with a larger range of uncertainty after the year 2100 (Figure 2.8). The SLR scenarios are based on different emission scenarios *(Representative Concentration Pathways, RCP)*, where RCP2.6 is a low-emission scenario and RCP8.5 a worst-case scenario. Until 2150 the likely range of global SLR is predicted to 0.4-0.7 m (RCP2.6) or 1-2 m (RCP8.5) relative to the mean sea level 1986-2005, the likely range lying in the middle 66 % probability span (IPCC, 2019).

The SLR relative to the land surface will not rise evenly all over the globe but experience regional variations. In Sweden, the post-glacial rebound will counteract the SLR and result in a lower relative SLR (Hieronymus and Kalén, 2020). The land-uplift varies within Sweden, where the north part generally experiences the largest uplift and the southern the least. In Ystad, the land uplift rate is 0.08 mm/yr (Nerheim, Schöld and Persson, 2017), which is not enough to counteract the SLR.

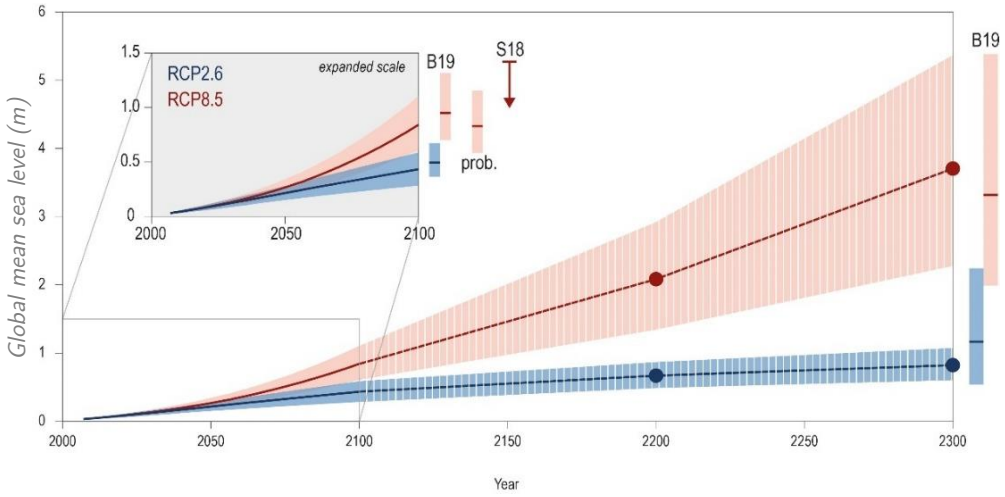

Figure 2.8: Projections for the global mean sea level in the future. Lighter colours indicate the likely scenario (66 % probability), blue is the low emission scenario RCP2.6 and red is the high emission scenario RCP8.5. Source: (IPCC, 2018).

The SLR scenarios describe the future mean water level. However, there is also the risk of extreme storm surges, which further elevates the sea level temporarily. Historically, high water levels of 2 m above mean sea level have been observed in Ystad (Nerheim and Johansson, 2018), and Dahlerus and Egermayer (2005) estimated the runup from storm waves during a 100-year event in Ystad just below 5 m (worst case scenario), which might increase in the future due to the changing climate.

2.4.1 Coastal Response to Sea Level Rise

Dean and Houston (2016) predict that accelerating SLR will become a more prominent factor in coastal response in the future. However, where much focus has been on determining future SLR, less has been on investigating the effects of said SLR (Cooper and Pilkey, 2004). In this thesis, variations of the hydrodynamic forcing are assumed unchanged, but rather the altitude at which they reach is changed. With SLR, the active forces will move upwards on the profile accordingly. Isolating the morphological impact of SLR from other factors, by looking at historical records, is difficult since so many factors are involved and interlinked (Cooper and Pilkey, 2004). However, the isolated

effects of SLR have been examined in laboratory experiments (Schwartz, 1967; Atkinson *et al.*, 2018), showing a recession of the shoreline. Field observations of shoreline retreat were made by Hands (1983) in the Great Lakes, US, where water levels rose by 1 m over a decade and induced an offshore sediment transport. However, the Great Lakes differ from the sea regarding, e.g., fetch size and presence of winter stratification. The first theoretical description of this SLR-induced shoreline recession was made by Bruun (1954), hereafter called the Bruun equilibrium concept, described in section 2.4.2. The finest sediment, e.g., silt and clay, tends to be removed from the system due to hydrodynamic forcings (Wolinsky and Brad Murray, 2009) and fine sands are deposited offshore but still within the active profile (Bodge, 1992; Rosati, Dean and Walton, 2013).

On the contrary, there are some examples of historical accretion during SLR, but only in places with a positive sediment budget (Schlager, 1993; Helland-Hansen and Hampson, 2009; Houston, 2015). Dean (1987) argued that the assumption that sand would only be eroded from the upper beach could not be the only truth. Combining the three presumptions that: 1) there is a long-term balance between on- and offshore forces creating the equilibrium profile, 2) accounting for the differences in grain size across the cross-shore profile and 3) that different grain sizes are stable at different depths, Dean concluded that the grains must move landwards during SLR to once again reach their equilibrium depth. This is called the Dean equilibrium concept and requires excess sand offshore the equilibrium profile that can be transported onshore by so-called Dean transport, and might also depend on SLR rate. The Bruun equilibrium concept is however the most common approach for SLR-induced coastal response, applicable when no excess material is present (Houston, 2015).

2.4.2 The Bruun Rule

The Bruun Rule is based on the Bruun equilibrium concept and is widely used in coastal management since it is the most commonly known simple-to-use method for shoreline recession estimations (Cooper and Pilkey, 2004). The model describes an equilibrium beach profile of a control volume that rises with SLR to re-establish the profile's position in relation to the new mean sea level (Figure 2.9). The equilibrium profile is then shifted landward, still

maintaining its shape until the control volume is the same as before SLR. The material needed to elevate the profile is eroded from the upper part of the profile, inducing a shoreline recession (Bruun, 1962). In this way, the Bruun Rule predicts a shoreline retreat parallel to the average slope of the active beach profile (Wolinsky and Brad Murray, 2009). When the equilibrium profile rises and migrates landward, a trailing ramp may be formed (Atkinson *et al.*, 2018), estimated to a slope of 1:12.5 based on model data (Vellinga, 1986), or to the average slope of the active profile (Dean, 1987). It can also be simplified as the ratio between SLR and the shoreline recession (Kriebel and Dean, 1993).

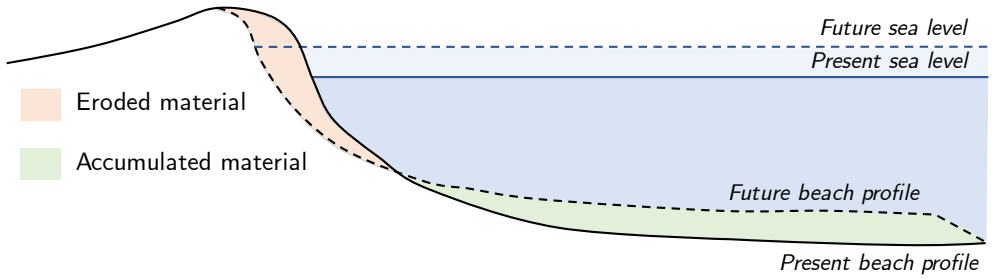

Figure 2.9: A cross-shore schematization of the principle of the Bruun Rule. The volume of eroded material (red) equals the volume of accumulated material (green), generating an upward and landward shift of the equilibrium beach profile.

There are several assumptions in the Bruun Rule, and its exclusive use has been criticised for not corresponding to natural beaches (Bruun, 1983; Thom, 1984; Cooper and Pilkey, 2004; Woodroffe *et al.*, 2012; Rosati, Dean and Walton, 2013; Cooper *et al.*, 2020), primarily since in reality many other factors are affecting the shoreline recession and sometimes overriding the Bruunian recession. In relation to the theory presented in this chapter, some relevant assumptions of the Bruun Rule are listed below (Bruun, 1962; Hallermeier, 1978; Dean and Maurmeyer, 1983; Davidson-Arnott, 2005):

- No gradient in longshore sediment transport rate is accounted for
- No other significant sources and sinks are regarded
- All sediment within the profile is transported in the offshore direction, with no transport across the DoC
- The profile is assumed to consist entirely of sand with uniform grain size and no variation in sediment sorting across the profile
- The sediment extends out to the DoC
- No consideration of inland topography, such as the dune system
- No local phenomena, like barrier islands, are considered

2.4.3 Developments of the Bruun Rule

Due to the numerous restrictive assumptions being discussed, there are several developments of the Bruun Rule, both for calculating the SLR-induced coastal response and introducing more factors affecting the future shoreline position.

Dean and Maurmeyer (1983) generalised the Bruun Rule to be applicable on barrier island migration. The generalised version includes the lagoon side parameters of the barrier island (active profile, DoC and berm height) in the standard Bruun Rule. Bruun (1988) showed that the original Bruun Rule could be modified to incorporate losses of sediments to underwater canyons or fine sediments offshore by introducing a "loss-function" dependent on a percentage of lost sediment or fine sediments. Rosati, Dean and Walton (2013) argued for the importance of sediment losses hinterland the beach, such as aeolian transport and overwash, and presented a modified Bruun Rule, including landward transport. The modification consists of an additive term, which would increase the beach recession, compared to the original Bruun rule, in the case of both seaward and landward transport.

Davidson-Arnott (2005) presented a conceptual model for shoreline migration, including the dune system in the model. The model is based on the same initial conditions as the Bruun Rule but assumes that the net cross-shore transport is landward, i.e., the lower part of the profile is eroded, and the sediment transported onshore. Furthermore, it assumes that all sediment eroded from the dunes are transported landward, causing the dune to migrate inland, maintaining its shape.

Edelman (1972) formulated a beach response model, considering the dune height. The dune face is assumed to be vertical, and the eroded sediment from the dune is spread out over the entire profile, which translates landward and upward in pace with SLR. The model was developed for erosion during storm conditions but is argued to be representative for long-term response as well (Dean and Maurmeyer, 1983). Young *et al.* (2013) presented a model for the erosion of cliffs fronted by sandy beaches. The model includes a non-uniform cliff composition and external sediment sources and sinks. The back beach acts as a sediment buffer which delays the cliff retreat.

Everts (1985) extended the Bruun Rule by introducing a term that includes other processes and activities affecting the coastal response, such as transport gradients in the longshore and cross-shore direction and sinks and sources, such as sand mining and beach nourishment. Similar models have been developed, for example, Stive, Nicholls and de Vriend (1991) and Dean and Houston (2016). Dean and Houston (2016) presented an additive model with terms each accounting for different coastal processes affecting the coastlines recession. The model includes the responses to SLR, cross-shore sediment transport, the gradient in longshore sediment transport and external sources and sinks, such as beach nourishment. Karunarathna *et al.* (2018) applied the model at the Sefton Coast, UK, and the results corresponded well to the observed historical shoreline change.

3 Case Study Site

Ystad Municipality, situated on the south coast of Scania has a coastline extending 40 km in an overall east-west direction, with the city of Ystad located in the middle (Figure 3.1). In Ystad, one of Sweden's largest harbours for cargo transport and ferries is located (Trafikverket, 2020). The area close to the coast holds various values, from infrastructure and businesses to recreation and wildlife that are in need of protection when the sea level rises. The sandy beaches along the coast are a popular tourist destination and are considered an important income source for the municipality. However, erosion has already caused problems at some beaches, and with rising sea levels, more sections of the coast are at risk (Ohlsson Skoog and Green, 2018).

The coastline within the municipality contains many different types of beaches. Small pocket beaches with poorly sorted material, from sand to boulders, dominate the coast west of Ystad. The nearshore zone mainly consists of clayey till covered by gravel and cobbles (Figure 3.2). The coastline east of Ystad is dominated by long beaches with fine sand, especially in Ystad Sandskog and from Löderups Strandbad to Sandhammaren (SGU, 2012; Malmberg-Persson *et al.*, 2016). In Ystad bay, the bottom material is dominated by sand along the shoreline, but further out, clayey till, gravel, and sand can be found. The nearshore bottom from Löderups Strandbad to Sandhammaren almost completely consist of postglacial fine sand (Figure 3.2). The bottom material outside Kåseberga ridge consists of coarse glaciofluvial deposits, sedimentary bedrock, and glacial till (Malmberg-Persson *et al.*, 2016). The nearshore wave climate outside the coast of Ystad municipality has incoming waves mainly from SW – E, with significant wave heights of up to 1.4 m being the most frequent (Adell *et al.*, 2021).

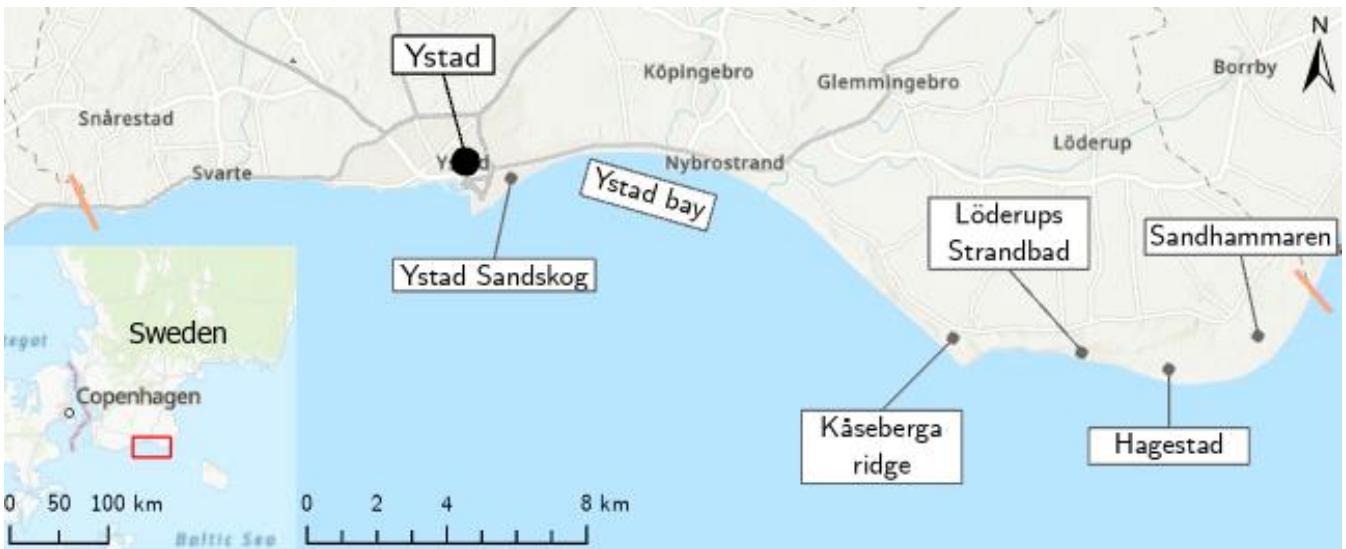

Figure 3.1: Map of Ystad municipality's coastline, delimited with orange lines, showing the main locations mentioned in this thesis. The overview map in the bottom left corner shows the location of Ystad municipality in Sweden.

Figure 3.2: Marine geology outside the coastline of the municipality. The largest area with sand is found outside the eastern part of the municipality. Data source: SGU (2019).

3.1 Erosion Problems and Protective Measures

Problems caused by erosion were observed in the municipality already in the late 19th century. Today, Ystad Sandskog and Löderups Strandbad are experiencing some of the worst erosion in Sweden (SMHI, 2018). For example, Löderups Strandbad was severely affected in the '60s and '70s, with two of the oldest houses being lost, and in the '90s, 150 campsites were lost due to a recession of 8 m (Ohlsson, 2008).

To compensate for the continued erosion in both Löderups Strandbad and Ystad Sandskog, the first large-scale beach nourishment project in Sweden was conducted, in addition to already existing hard structures. The initial nourishment was performed in 2011, with renourishments in 2013, 2017 and 2020, with volumes used presented in Table 3.1. The sand was distributed

along one uniform section of the coast in Sandskogen and divided between smaller sections in Löderups Strandbad (Skoog, 2020). In addition to only prevent the coast from erosion-related damages, the beach nourishment also restores recreational values associated with the beaches. The last renourishment has not been evaluated yet, but a positive effect can be seen based on the increase in sediment volume both on the shore and in the nearshore area (Skoog, 2020).

Table 3.1: Volumes of sand added during the beach nourishments in Sandskogen and Löderups Strandbad (Skoog, 2020).

Year	Ystad Sandskog V (m3)	Löderups Strandbad V (m3)
2011	72 870	23 632
2014	64 108	16 112
2017	53 227	27 077
2020	56 760	24 443
Total	246 965	91 264

In Löderups Strandbad, the coastline has retreated 200 m since 1960 (SMHI, 2018), which has caused the destruction of properties and forced residences to retreat further inland (Hanson and Almström, 2013). Measures have been taken to reduce the erosion and protect the coastline. The coastline has been reinforced with rocks, and six groynes have been constructed during different periods in the 20th century, seen as lines perpendicular to the beach in Figure 3.3. However, the protections did not entirely solve the erosion problems. The rocks moved the erosion from the shoreline to the shallow bottom instead, undermining the structures, and the groynes are suspected to obstruct the longshore sediment transport, causing erosion east of the village instead (Ohlsson Skoog and Green, 2018). As a result, the coastline in the western part is stable but has lost its beaches. The beaches are still present in the eastern part, but the coastal recession has accelerated, seen in Figure 3.4.

Figure 3.3: Overview of Löderups Strandbad. The rock-reinforced coastline is visible as the section where no beach can be seen. The groynes are seen as the lines perpendicular to the shoreline. Source: Scalgo Live (n.d)

Figure 3.4: Picture taken at the west part of Hagestad nature reserve, in the west direction with Kåseberga ridge and Löderups Strandbad in the background. Indicated with yellow arrows are one of the groynes and signs of erosion. Photo: Elin Olsson

In Ystad Sandskog, the major part of the erosion occurs below the water surface (Hanson and Almström, 2013), but erosion is also visible in the vegetation line at some sections (Ohlsson Skoog and Green, 2018). The future erosion in combination with high-water levels and over-wash of the dunes threatens both the valuable beaches and the properties and infrastructure behind the beach. Due to this, several different protective measures have been implemented at Ystad Sandskog, seen in Figure 3.5. Sections of the coast have been reinforced with revetments in combination with five detached breakwaters and five groynes. The retreat of the coastline in between and downdrift some of the groynes, before the beach nourishment occurred, indicated that solely the hard protection measures were not enough to protect the coast from erosion (Borell Lövstedt and Persson, 2015; Ohlsson Skoog and Green, 2018). However, the combination of groynes and the beach nourishment (extending from 'Idrottsplatsen' to groin B_4) has worked well. Most of the nourished materiel has stayed within the nourishment area and the portion that has 'escaped' to the east was later trapped by the detached breakwaters V_1 to V_5 (Hanson, H., 2021. Personal communication).

Figure 3.5: Overview of Ystad Sandskog. The groynes are seen as lines perpendicular the coastline, marked $B_0 - B_4$, and the detached breakwaters are seen as small dots in the upper right corner, marked $V_1 - V_5$. The beach nourishment has been placed in the grey and light yellow areas. The harbour lies west of 'Idrottsplatsen'. (Source: Hanson, H., 2021. Personal communication)

4 Methodology and Data

This chapter presents the equations and methods used in this study and the available data sources used. Section 4.1 describes how the geographic areas for model application were selected, section 4.2 present the methodology used to determine the extent of the active profile, and section 4.3 introduces the different models used and their assumptions. The available data are presented in section 4.4. Finally, section 4.5 and 4.6 describes the sensitivity analysis and Monte Carlo simulations performed.

4.1 Areas for Model Application

For the model applications, four transects along the coast of Ystad municipality were selected. The selection was based on two initial criteria: (1) The surface material should consist of sand within the active profile, and (2) the profiles should display different long-term evolutions; accreting, eroding and stable. As a first step, marine and beach geology were investigated (SGU, 2019). Areas, where the marine sediment was dominated by other materials than sand were excluded. As a second step, the historical coastline evolution during the period 1960 – 2012 was studied using the results from a digital vegetation line analysis by Fredriksson *et al.* (2017). Thirdly, three transects with different erosion/accumulation trends were chosen to investigate the effect of SLR on the total shoreline change. In addition, one transect was chosen where coastal protection measures are present.

4.2 The Active Profile

The DoC of the active profile was calculated using a method developed by Hallermeier (1978) (4.1)) where the DoC is a function of wave properties:

$$h_{dc} = 2.28H_{S,eff} - 68.5\left(\frac{H_{S,eff}^2}{gT_{m,eff}^2}\right) \tag{4.1}$$

where h_{dc} is the DoC, $H_{S,eff}$ and $T_{m,eff}$ is the effective significant nearshore wave height and effective mean wave period, respectively, defined as the mean significant wave height and period exceeded only 12 hours per year

(Hallermeier, 1978). It is calculated as the significant wave height and mean wave period of the upper 0.14-percentile of the wave record (Dean and Dalrymple, 2004).

The subaqueous profile width was primarily calculated using the Dean profile (Equation (4.2)). In addition, the width was estimated using nautical charts, bathymetry data and profile records from repeated measurements (Hanson, 2014) to compare with the Dean profile.

$$h_{dc} = Ax^{2/3} \tag{4.2}$$

where x is the horizontal distance from the shoreline to DoC and A is a scale parameter, principally depending on median grain size. The scale parameter is a function of the fall velocity according to Equation (4.3) (Dean, 1987):

$$A = 0.067w^{0.44} \tag{4.3}$$

where w is the fall velocity of a grain in cm/s. The fall velocity was calculated using Equation (4.4) proposed by Sadat-Helbar *et al.* (2009). The relation was chosen since the study examined 22 different fall velocity relations and verified the proposed relation with laboratory data.

$$w = \begin{cases} 0.033\dfrac{\upsilon}{d}\left(\dfrac{d^3 g(s-1)}{\upsilon^2}\right)^{0.963} & D_{gr} \leq 10 \\ 0.51\dfrac{\upsilon}{d}\left(\dfrac{d^3 g(s-1)}{\upsilon^2}\right)^{0.553} & D_{gr} > 10 \end{cases} \tag{4.4}$$

where υ is the kinematic viscosity of water, d the grain size (in this study d_{50} is used), g the gravitational constant, s the relative density of the sediment and D_{gr} the effective diameter calculated as:

$$D_{gr} = d\left(\frac{g(s-1)}{\upsilon^2}\right)^{\frac{1}{3}} \tag{4.5}$$

The landward limit of the active profile was assumed to be the dune foot since it is relatively stable over time, meaning that the timing of topography measurements is negligible. The berm height *(B)* was defined as the dune foot elevation, estimated from elevation profiles. The dry beach width, between the dune foot and shoreline, was measured on several aerial photos using the average value as input. A summary of the data used is presented in Table 5.1.

4.3 Model Descriptions

Four models were selected for the computations, in addition to the Bruun Rule. The selection of models gives a more diverse picture than the Bruun Rule alone, but all processes affecting the shoreline are not represented. However, the models are chosen to be suitable for the conditions present in the study area. The four models can be divided into two groups based on the way they differ from the Bruun Rule, according to Figure 4.1.

The first group of models is a development of the morphological response to SLR by including the dune system in the analysis. The models within this group are:

- Edelman II model, by Edelman (1972)
- The Dune Models, developed within this study.

The second group consists of extended versions of the original Bruun Rule, which considers additional transport processes affecting the shoreline recession, and contains:

- The Dean & Houston model (DHM), by Dean and Houston (2016)
- Model for the longshore spread of beach nourishment, by Pelnard-Considere (1956) and Dean (2002).

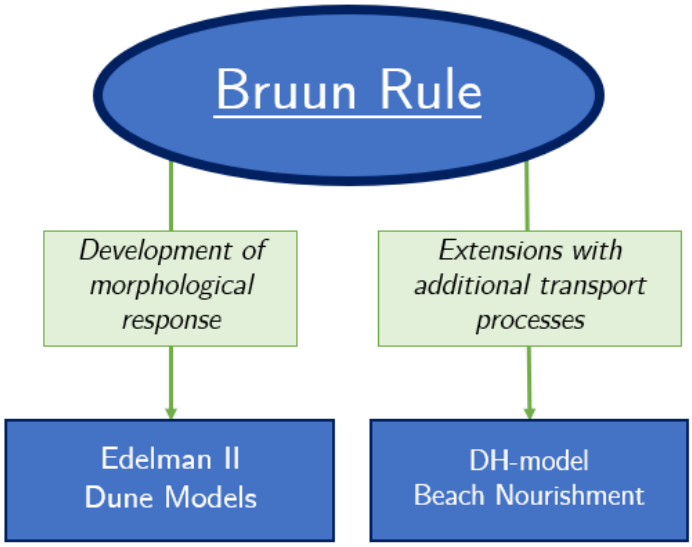

Figure 4.1: The two groups of models used. One group accounts for additional transport processes affecting the shoreline recession while the other group is a development of the Bruun Rule and the morphological response to SLR.

These models were chosen since they have an easily applicable approach, similar to the Bruun Rule, and they account for some of the limiting assumptions in the Bruun Rule. Regarding the available data and site-specific conditions, the models are also suitable for the study site. The models are more thoroughly described in the following sections.

4.3.1 The Bruun Rule

The Bruun Rule (presented more in detail in section 2.4.2) is based on the Bruun equilibrium concept and estimates the shoreline recession caused by SLR (Bruun, 1962; Dean, 1991). The shoreline recession (R) is given by:

$$R = -S\frac{W_P}{h_{dc} + B} \tag{4.6}$$

where S is the SLR, W_P the subaqueous profile width, h_{dc} the DoC and B the berm height.

To adjust to the SLR and maintain the equilibrium state, the profile is elevated at the same rate. The material needed to raise the profile is eroded from the upper part of the profile, thus generating a recession of the shoreline (Figure 4.2).

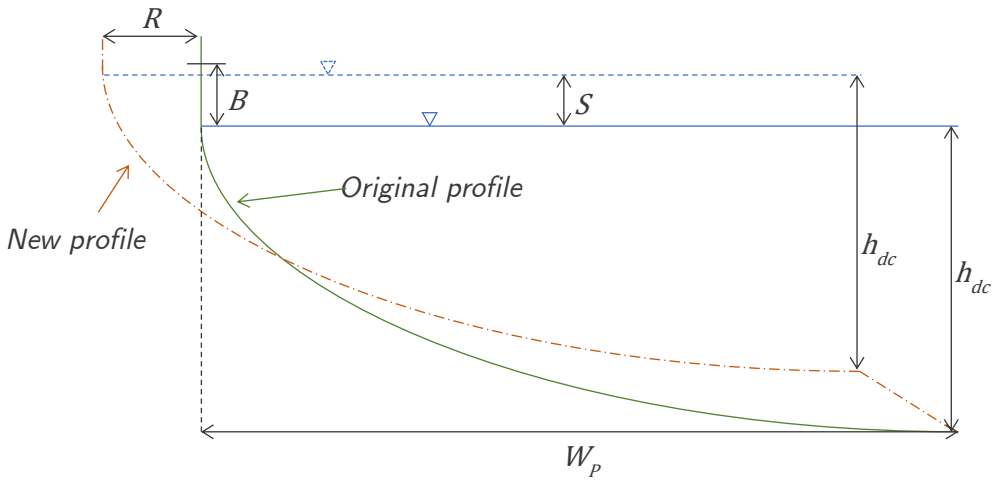

Figure 4.2: Shoreline response to SLR according to Bruun Rule. The green line represents the original profile before SLR and the orange line shows the position of the profile after SLR.

In this study, the berm height is assumed to be the dune foot elevation, and thus the Bruun Rule equation includes the width of the dry beach (W_B) in addition to the subaqueous profile width, as in Equation (4.7).

$$R = -S\frac{W_P + W_B}{h_{dc} + B} \tag{4.7}$$

4.3.2 Edelman II

The beach response model formulated by Edelman (1972) is similar to the Bruun Rule by assuming the rise of the profile with SLR. However, the Edelman II method also includes the dune height relative to the mean sea level by subtracting the SLR, seen in Equation (4.8) and Figure 4.3.

$$R = L \cdot ln\left(\frac{h_{dc} + B_0}{h_{dc} + (B_0 - S)}\right) \tag{4.8}$$

where B_0 is the dune height, and L is the width of the active profile, which in this analysis is assumed to include the beach width. The sediment needed to raise the profile is assumed eroded from the beach and the dunes. While the sea level rises, the relative dune height decreases, assuming no aeolian build-up. This generates a greater relative erosion as the sea level rises since less material is present in the dunes (Dean and Maurmeyer, 1983).

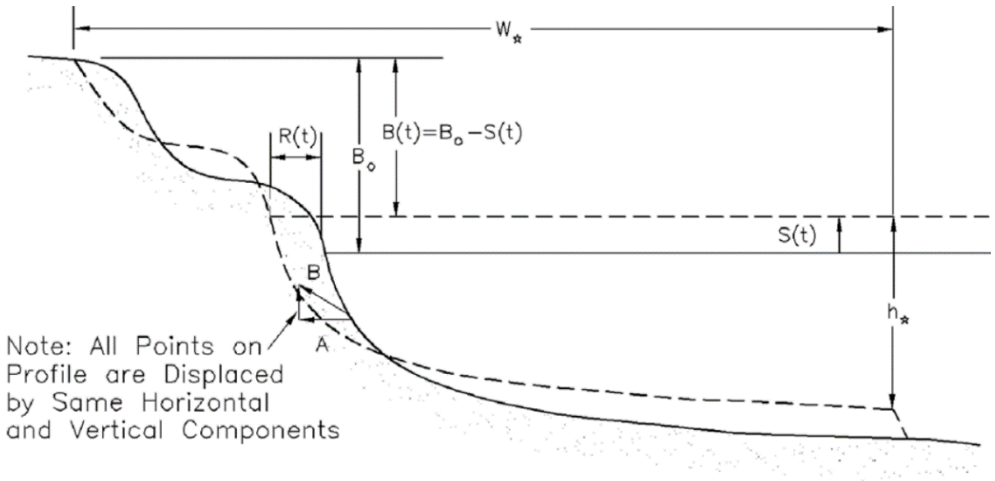

Figure 4.3: Illustration of the Edelman II method The dotted profile is after SLR when the profile is elevated by S m and migrated inland R m. The dune elevation is unchanged, but the relative dune height, B(t), is diminished. h_* is the DoC.

4.3.3 Dune Models

In this study, a modified Bruun Rule was developed to include the dune system, inspired by methods developed by both Hanson (2021, personal communication) and Kriebel and Dean (1993). It is based on the calculation of cross-shore section areas before and after SLR and is iterative to obtain the shoreline recession (*R)*. Three versions of this method were developed and are described in this section. The versions are:

1) Dune Model – Basic
2) Dune Model – Topography
3) Dune Model – Usable sand

In addition to the basic assumptions of the Bruun Rule, it was assumed that:

- The beach profile extends landward beyond the dune foot.
- The active profile is assumed to extend from the DoC until the dune foot, as for the Bruun Rule, and the dune face slope is assumed to stay the same.
- The dune top has reached a maximum elevation.
- The dune will not retreat landward during SLR since vegetation on the dune is assumed to reduce the aeolian transport and stabilise the dune.

The dune models could be extended to also include an imbalance in sediment budget by using Equation (4.9). It has not been done in this study since the erosion and accumulation is investigated with the Dean & Houston model (Section 4.3.4).

$$a_{old} = a_{new} + storage \tag{4.9}$$

Where a_{old} and a_{new} are the cross-shore section area before and after SLR, respectively, and *storage* is the positive change in sediment budget.

The first Dune Model developed was the Dune Model – Basic, where the dune was simplified to a rectangular shape with no beach plane present, see Figure 4.4. To describe the profile before and after SLR, equation (4.10) and (4.11) were used, respectively.

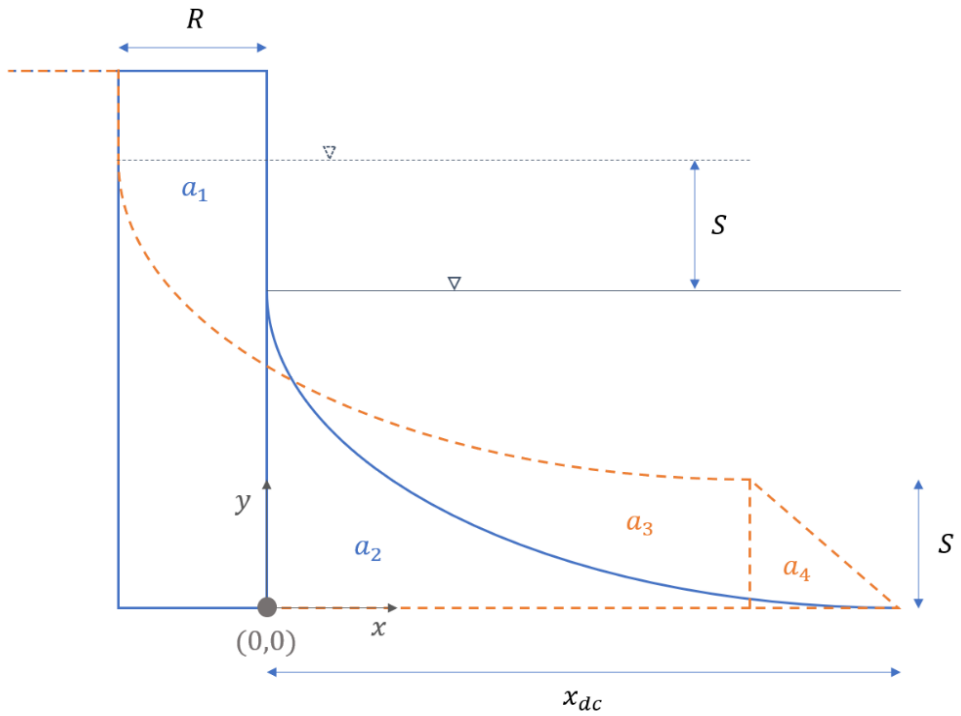

Figure 4.4: Schematic picture of the Dune Model – Basic. The blue and orange profiles represent the position before and after SLR respectively. The blue areas are assumed equal to the orange areas.

$$y = \begin{cases} h_{dune} + h_{dc}, & x < 0 \\ h_{dc} - A \cdot x^{2/3}, & x > 0 \end{cases} \tag{4.10}$$

$$y = \begin{cases} (h_{dc} + S) - A(x + R)^{2/3}, & x < x_{dc} - R \\ \frac{S}{R}(x_{dc} - x), & x > x_{dc} - R \end{cases} \tag{4.11}$$

Where h_{dune} is the dune height, x the horizontal distance from the original shoreline, y the vertical distance from DoC and R is the shoreline recession, initially set to zero and increased for every iteration. After each iteration, the profile was moved landward R m, and the areas under the old and new profiles were calculated according to Equation (4.12) - (4.15). See Figure 4.4 for reference.

$$a_1 = (h_{dune} + h_{dc})R \tag{4.12}$$

$$a_2 = \int_0^{x_{dc}} \left(h_{dc} - A \cdot x^{\frac{2}{3}}\right) dx \tag{4.13}$$

$$a_3 = \int_{-R}^{x_{dc}-R} \left((h_{dc} + S) - A(x + R)^{2/3}\right) dx \tag{4.14}$$

$$a_4 = \frac{S \cdot R}{2} \tag{4.15}$$

The iterations were continued until the areas were equal, as in Equation (4.16):

$$(a_1 + a_2) - (a_3 + a_4) = 0 \tag{4.16}$$

The second Dune Model developed was the Dune Model – Topography, aiming to adapt the Dune Model – Basic better to site-specific dune topography. To calculate the shoreline recession, the following steps were performed:

1) A dune elevation profile with (x,y)-coordinates was joined to the subaqueous profile (Equation (4.2)) at the waterline (Figure 4.5a).
2) The y-axis was adjusted to start at the DoC, as in the Dune Model – Basic.
3) The profile seaward of the dune top was raised a vertical distance corresponding to the SLR but until maximised by the original dune top elevation (Figure 4.5b).
4) The elevated profile was moved an initial distance ($R_{initial}$) to intersect with the non-elevated dune profile (Figure 4.5b).
5) At the seaward end of the profile, a trailing ramp with slope S/R was implemented (Kriebel and Dean, 1993).
6) The raised profile was moved landward with steps of 0.1 m util the integrated areas before and after SLR were equal (Figure 4.5c).
7) The shoreline recession (R) was calculated by summation of every iteration step.

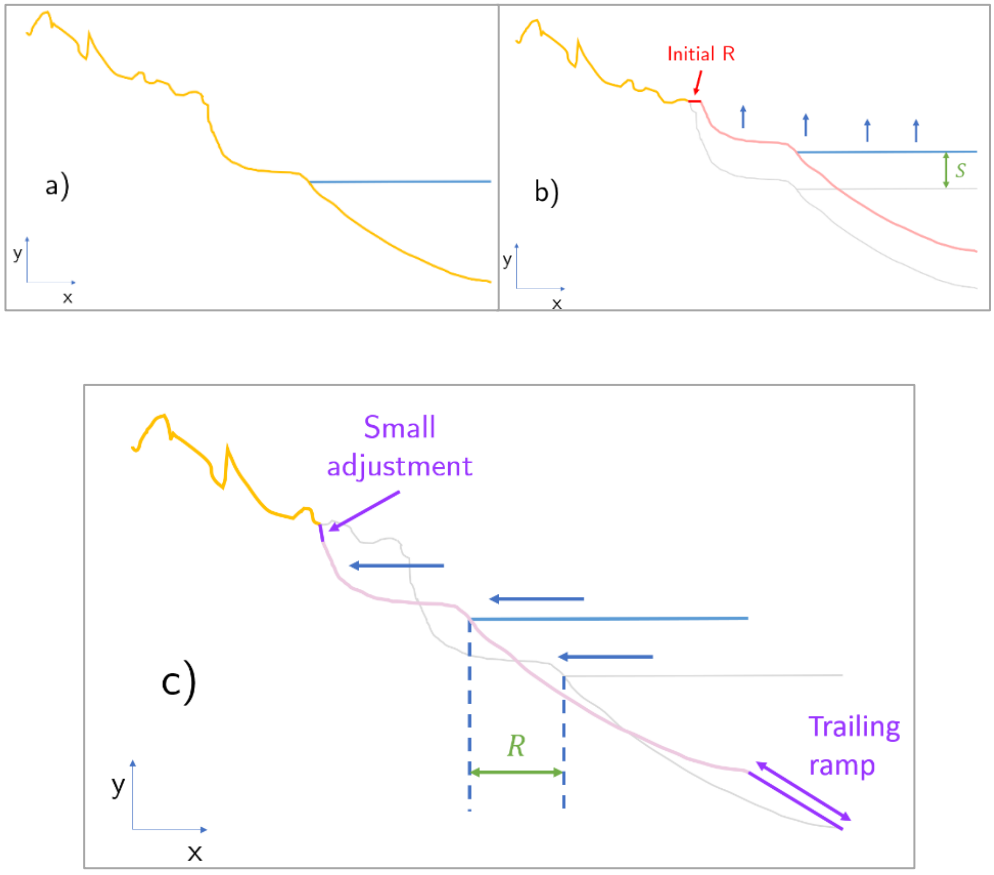

Figure 4.5: Schematized modelling steps of the Dune Model – Topography. a) shows the initial profile, in b), the profile is elevated by the SLR and the horizontal, red part initial R is later removed and in the final step c) the profile is finally moved landward until the areas (including the total subaqueous profile) equal zero. The small adjustment (purple) is due to the dune elevation being lower than the inland elevation. At the bottom end of the profile, a trailing ramp (purple) is introduced. The grey profiles in b) and c) are the initial profile in a). The subaqueous profile is largely under dimensioned.

Finally, a third method was developed: Dune Model – Usable Sand, to account for the fraction of sand in the eroding dunes compatible with the active profile material. This excludes clay lenses, roots, other fine materials that will be washed away or other non-compatible materials (Dean and Maurmeyer, 1983). Larger objects, such as rocks, are not considered in this model since they are, if present, not likely to be washed away and thus not contribute to elevating the subaqueous profile. If all the eroded material from the dunes is compatible, the fraction of usable sand is set to equal one.

Due to the geometry in this model, it is most suitable for profiles where the inland is relatively flat until there is a steeper slope down onto the beach. The subaqueous profile was set to the Dean profile (Equation (4.2)) plus the dry beach. In Figure 4.6, the active profile is simplified to a triangle since these areas are the same before and after SLR. In the model, the area under the beach profile was divided into subsections, and the sections above the initial dune foot were assigned the fraction of usable sand (Figure 4.6).

The relation between dune and shoreline recession is described in Equation (4.17).

$$R = R_{dune} + (x_{11} - x_{21}) \tag{4.17}$$

R_{dune} is the dune recession and R is the shoreline recession. x_{11} and x_{21} are the horizontal distances between the dune top and dune foot before and after SLR, respectively.

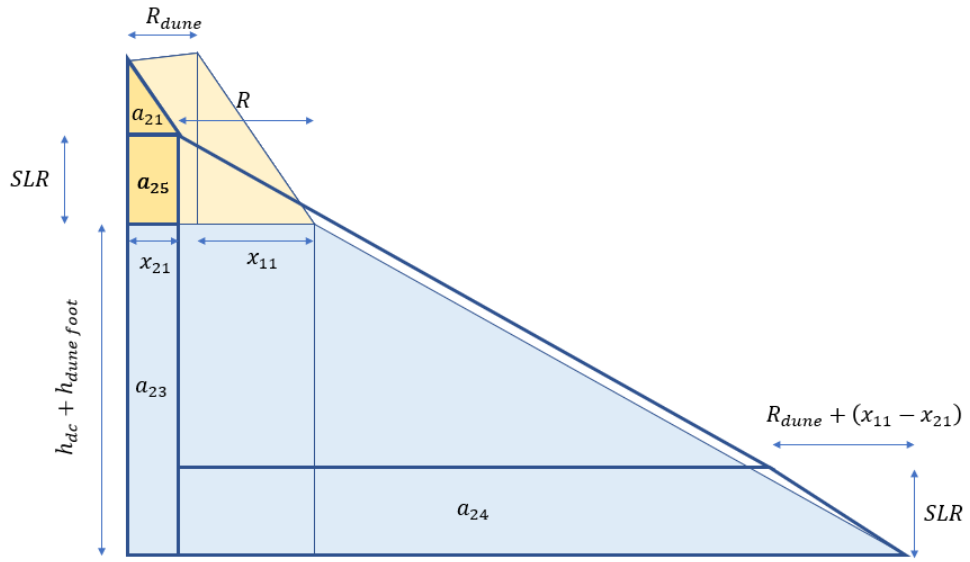

Figure 4.6: Dune Model - Usable Sand. The yellow areas represent the erodible volume assigned the fraction of "usable sand". The equilibrium profile is simplified to a straight line since the areas are the same before and after and cancel each other out.

4.3.4 Dean Houston Model

The model for shoreline change proposed by Dean and Houston (2016), hereafter referred to as DHM, combines shoreline recession caused by SLR with the shoreline's response to longshore sediment transport rate gradients, onshore sediment transport as well as sinks and sources according to Equation (4.18):

$$\frac{dR}{dt} = -\frac{dS}{dt}\left(\frac{W_*}{h_{dc}+B}\right) + \frac{\phi}{h_{dc}+B} - \frac{1}{L(h_{dc}+B)}\frac{dV_{sink}}{dt} + \frac{1}{L(h_{dc}+B)}\frac{dV_{source}}{dt} - \frac{1}{(h_{dc}+B)}\frac{dQ}{dy} \tag{4.18}$$

The different parameters in Equation (4.18) are presented in Table 4.1.

Table 4.1: Variables in DHM

R	[m]	Shoreline change	V_{sink}	[m³]	Sand volume removed from the system
S	[m]	Sea level rise	V_{source}	[m³]	Sand volume added to the system
W_*	[m]	Width of profile	L	[m]	Length of coast affected by the sink/source
h_{dc}	[m]	Depth of closure	$\frac{dQ}{dy}$	$\left[\frac{\text{m}^3}{\text{m}\cdot\text{yr}}\right]$	Longshore sediment transport gradient
B	[m]	Berm height	t	[yr]	Time
ϕ	$\left[\frac{\text{m}^3}{\text{m}\cdot\text{yr}}\right]$	Onshore transport rate			

The sink term (ΔV_{sink}) could include inland aeolian transport and removal of dredged material from the active profile, while the source term includes, e.g., beach nourishment volumes.

Conservatively assuming onshore transport (Φ) to be negligible over the studied period (150 years) and that no sinks are present, Equation (4.18) can

be integrated over the time Δt, yielding equation (4.19). In addition, the longshore transport gradient was assumed to be constant over the years.

$$\Delta R = -\Delta S\left(\frac{W_*}{h_{dc}+B}\right)+\frac{\Delta V_{source}}{L(h_{dc}+B)}-\frac{dQ}{dy}\frac{\Delta t}{(h_{dc}+B)} \tag{4.19}$$

In DHM, the added beach nourishment volume is assumed continuous over the whole profile and time series, i.e., the total sand volume added is evenly spread over the profile and years. In addition, the added sand is assumed to remain within the beach profile over the entire period. However, in reality, the sand volume added to a system during a beach nourishment occurs as a unit load at a time step and spreads out over time, both in cross- and longshore direction.

4.3.5 Longshore Spread of Beach Nourishments

To account for the variations over time of a beach nourishment, another modelling approach was investigated. It was done by adding unit loads at specific time steps in two different time-dependent diffusivity equations. The added sand will then spread out according to the diffusivity equations, and the shoreline recedes slightly from the initial position. The beach nourishment model is then extended to include SLR effects by adding a term of Bruunian shoreline recession. In addition, an equation accounting for the influence of a groyne on beach nourishment was included.

The equations calculate the cross-shore position of the shoreline but consider the longshore development over time. The equations can also describe the longshore development of the beach nourishment, but in this study, the longshore distance, x, was kept constant. To be able to compare the equations, the diffusivity was kept constant.

The first longshore spread equation used was derived by Pelnard-Considère (1956). The equation describes an elementary plan view of a once added, bell-shaped beach nourishment and its development over time in the cross-shore direction according to:

$$y = \frac{a}{2\sqrt{\pi\varepsilon t}} e^{-\frac{x^2}{4\varepsilon t}} \tag{4.20}$$

Where y is the cross-shore distance from the unnourished shoreline and x the longshore distance from the centre of the nourishment. ε is the longshore diffusivity, determined conservatively based on breaking wave height presented by Dean (2002) (Table A.1). The breaking wave height *(H_b)* was roughly calculated by Equation (4.21) with an estimated breaking depth *(h_b)* at 1.5 m.

$$H_b = 0.78 h_b \tag{4.21}$$

Furthermore, the profile of interest was assumed to be located at $x = 0$ and the sand instantly distributed uniformly across the profile. The area, a, was calculated by the beach nourishment volume divided by the potential thickness of the nourishment (assumed to be 1.5 m).

The second longshore spread equation used describes the development of an initially rectangular beach fill (Dean, 2002):

$$y = \frac{y_0}{2}\left\{erf\left[\frac{l}{4\sqrt{\varepsilon t}}\left(\frac{2x}{l} + 1\right)\right] - erf\left[\frac{l}{4\sqrt{\varepsilon t}}\left(\frac{2x}{l} - 1\right)\right]\right\} \tag{4.22}$$

$$erf(z) = \frac{2}{\sqrt{\pi}} \int_0^z e^{-u^2} du \tag{4.23}$$

where y_0 is the shoreline's position directly after the beach nourishment, compared to the unnourished shoreline, set to the same initial y as for the bell-shaped beach nourishment. x is the longshore position of the transect, assumed to be located in the centre of the rectangle, thus set to zero. ε is the longshore diffusivity. l is the length of the nourishment and t the time.

The error function is a mathematical equation giving the probability that a random variable falls within the interval $[-z, z]$, in this case, z equals:

$\left[-\frac{l}{4\sqrt{\varepsilon t}}\left(\frac{2x}{l}+1\right), \frac{l}{4\sqrt{\varepsilon t}}\left(\frac{2x}{l}+1\right)\right]$ or $\left[-\frac{l}{4\sqrt{\varepsilon t}}\left(\frac{2x}{l}-1\right), \frac{l}{4\sqrt{\varepsilon t}}\left(\frac{2x}{l}-1\right)\right]$,

for a normal distribution with mean 0 and variance ½, since it is the integration of the normal distribution curve (Weisstein, no date).

The third equation used describes the shoreline's evolution in the proximity to a groyne in time and space, derived by Pelnard-Considère (1956). This equation was included since the presence of a groyne will influence the spread of a nourishment.

$$y = \begin{cases} \pm\left[\sqrt{\frac{4\varepsilon t}{\pi}}\, e^{-\frac{x^2}{4\varepsilon t}} - |x| erfc\left(\frac{|x|}{\sqrt{4\varepsilon t}}\right)\right] tan(\alpha_0), & y < l_{groyne} \\ \pm\, l_{groyne} \cdot erfc\left(\frac{|x|}{\sqrt{4\varepsilon t}}\right), & y > l_{groyne} \end{cases} \quad (4.24)$$

Where l_{groyne} is the length of the groyne, x is the longshore distance from the groyne, and α is the angle between the approaching wave crest and the initial shoreline. The $+$ depends on whether the examined profile lies on the accumulating or eroding side of the groyne. In the studied case, the nourished profile is located on the accumulating side. Sediments will accumulate on the updrift side of the groyne until $y = l_{groyne}$, after that it will pass the groyne and continue to spread downdrift the groyne in the longshore direction. Equation (4.24) was added as a term to the shoreline position after initial beach nourishment.

4.4 Available Data

The data used to estimate the input values to the calculations are presented in Table 4.2. More detailed descriptions of the median grain size, SLR and longshore transport data are given below.

Table 4.2: Data sources used to estimate input values to the calculations

Data	Source	Type
Significant wave height and peak wave period	Adell *et al.* (2021)	Wave hindcast model 1979 - 2019
Median grain size	Berin and Löwdin (2021) (Schmidt, 2016)	Beach sediment samples
Measured beach width	Lantmäteriet (no date) TerraMetrics (no date) SCALGO Live (no date)	Orthophotos
Measured subaqueous profile width	EMODnet Bathymetry Consortium (2020) Malmberg-Persson *et al.* (2016) Sjöfartsverket (2015)	Bathymetry (115x115 m) Bathymetry, (2x2 m) Nautical charts
Profile records	Hanson (2014)	Profile measurements, 16 measurements 1997-2015
Future SLR	IPCC (2019)	RCP2.6 and RCP8.5 used
Historic SLR	SMHI (2021)	Observed water levels in Ystad
Berm- and dune height	Lantmäteriet (2021)	New National Elevation model, resolution 1x1 m
Longshore transport gradients	Fredriksson et al. (2017)	Digital vegetation line analysis 1960-2012
Beach nourishment data	Skoog (2021)	Volumes and nourished areas
Marine geology	SGU (2019)	Web application
Beach geology	SGU (2019)	Web application

The grain size data, provided by Berin and Löwdin (2021), contained grain size samples taken in the Bascom point (Bascom, 1951), calculated median grain size, and sample locations. In this study, the median grain size from the most adjacent sample location to each selected profile was used as input value to the calculations. Where no nearby measurement was available, the median grain size was estimated from the average value between the two most nearby sampling locations.

The SLR between 2000 and 2150 was obtained by digitising the projections by IPCC (2019) presented in Figure 2.8 by using the MATLAB package GRABIT and fitted to a polynomial. The global projections were used since no regional projections for Ystad in the year 2150 were available, and the projected global SLR were close to the regional SLR in 2100 (SMHI, 2020a). The land uplift in Ystad (0.08 mm/yr) was then subtracted from the global SLR to obtain the relative SLR, finally resulting in Equation (4.25) and (4.26).

$$\text{RCP2.6} \qquad S = (-8.33 \cdot 10^{-6} t^2 + 4.99 \cdot 10^{-3} t) - 0.08 \cdot 10^{-3} t \tag{4.25}$$

$$\text{RCP8.5} \qquad S = (-2.12 \cdot 10^{-7} t^3 + 8.47 \cdot 10^{-3} t^2 + 1.87 \cdot 10^{-3} t) - 0.08 \cdot 10^{-3} t \tag{4.26}$$

where S is the SLR in meters relative to mean sea level 1986 – 2005 and t years after 2000.

The gradients in LST were estimated from an analysis of the vegetation line's position in 1960 and 2012 from aerial photographs (Fredriksson *et al.*, 2017). The contribution from SLR to the total change 1960 – 2012 was then calculated using the Bruun Rule with SLR-observations from SMHI (2021) and subtracted from the total change in the vegetation line's position. Finally, the yearly change was obtained by dividing the total change by the time (Equation (4.27)). The resulting change in shoreline position per year was used as the LST-gradient term of the DHM, assumed constant for the studied period.

$$\frac{1}{(h_{dc} + B)} \frac{dQ}{dy} = \frac{R_{total,1960-2012} - R_{Bruun,1960-2012}}{t_{1960-2012}} \tag{4.27}$$

The high-resolution bathymetry was classified in the eastern part of the municipality's coast and could not be accessed. However, both grain size data from Schmidt (2016) and high-resolution bathymetry data from Malmberg-Persson *et al.* (2016) were available at Knäbäckshusen, eastern Scania. Therefore, a comparison between the calculated and measured profile width was performed on a beach profile at the Knäbäckshusen.

4.5 Sensitivity Analysis

A sensitivity analysis was performed for the Bruun Rule, including the calculation of the profile width and DoC, to investigate how sensitive the model is to changes in the input parameters. The input parameters were adjusted + 25 % one at a time, and the resulting change in shoreline recession was plotted versus the interval of the parameters. The results of the sensitivity analysis indicate the parameters in most need of a narrow estimation interval to reduce the uncertainty of the calculated recession.

Since there are many ways to estimate the subaqueous profile width, a comparison between the shortest and longest estimated profile widths was performed to quantify the difference in the resulting recession.

4.6 Monte Carlo Simulation

A Monte Carlo (MC) simulation was performed to assess the variation in the predicted recession caused by uncertainty in the input data for the Bruun Rule and DHM. Each input parameter was estimated as an interval rather than a fixed value and assigned a probability distribution. The MC model first generated an interval for the width of the active profile and then calculated the shoreline recession 10 000 times. Each calculation was performed with a new random set of values within the given probability intervals, and the output was generated as a probability interval of the shoreline recession, based on the input intervals and probability distribution.

The purpose of the MC simulation was to visualise the uncertainty in the calculated recession, rather than to investigate how different probability distributions of the intervals affect the results, and the data used was too

scarce to determine the mean and standard deviation. Due to this, the probability distribution assigned was either uniform or triangular. The uniform probability distribution only requires the lower and upper limit of the interval to be specified, and the values within the interval are equally likely to be observed. For the triangular distribution, a most likely value needs to be set in addition to the limits. The uniform distribution was assigned to the intervals for which a most likely value could not be determined based on the available data, i.e., the dry beach width and the berm height. The remaining intervals were assigned the triangular probability distribution. The input intervals were estimated based on available data (Table 4.2), and the methods used are presented in Table 4.3.

Table 4.3: Probability distribution and method used to estimate the input intervals to the MC simulation. (U) and (T) represents the intervals assigned the uniform and triangular probability distribution, respectively.

Interval		Method to estimate the interval limits
SLR	(T)	IPCC's (2019) likely range of SLR for RCP8.5
Scale parameter	(T)	Most likely and limits calculated from d_{50} in closest and adjacent sampling locations, respectively
Dry beach width	(U)	Lowest and largest measurements obtained from aerial photographs
Berm height	(U)	The highest respectively lowest points where the dune foot could be considered to be located based on elevation profiles
Effective significant wave height	(T)	$\pm$0.5 m from the effective significant wave height estimated from wave records
Effective mean wave period	(T)	$\pm$0.5 s from the effective significant wave height estimated from wave records
Shoreline change from LST-gradients	(T)	+0.5 m on the value obtained from the vegetation line analysis

Due to uncertainties in the assumption of probability distributions and the intervals, the two parameters most affecting the results were assigned a normal distribution in a new run to compare the results. The normal distributions

were designed to assimilate the estimated probability intervals in Table A.2, with mean values as the most likely values and tails extending further than the interval limits, giving a smoothing effect. The two parameters chosen were the A-parameter and the SLR parameter. The SLR was assigned the standard deviation (STD) 0.266 in accordance with the lowest possibility of the likely range of IPCC (2019), and the STD of the A parameter was estimated to 0.01.

5 Results and Discussion

Section 5.1 presents areas where the Bruun Rule is applicable within Ystad Municipality, the characteristics of the selected beach profiles and a discussion concerning the profile width. Section 5.2 - 5.5 present the results from the different models applied. The values for shoreline recession presented cannot be assumed to correctly represent the actual future recession due to uncertainties in the data. However, in this study, the recession is presented as exact values to be able to compare the different methods. The comparison is presented in section 5.6, followed by an alternative approach for presenting the results in section 5.7, accounting for uncertainties.

5.1 Beach Profiles

Presented below are the results of the Beach profile selection, based on the applicability of the Bruun Rule, model input data assessment, and the discussion regarding the profile width.

5.1.1 Geographic Applicability of the Bruun Rule

Investigation of the marine and beach sediments within Ystad municipality (from SGU, 2019) shows that the Bruun Rule is only applicable on approximately 10 km of the 40 km long coastline (Figure 5.1), based on the assumption that the surface material should consist of sand within the active profile. Combined with the Bruun Rule assumption of a net-zero sediment budget, the number of areas where the Bruun Rule alone can be used for accurate projections is further reduced (Figure 5.2).

However, two areas with historical erosion and accretion were chosen for one of the objects of this thesis: to compare the SLR-induced erosion to other coastal processes. One transect with a relatively low sand availability was also chosen to investigate the effect of not having enough sand, and also to investigate the beach nourishments conducted at the site. These investigations resulted in the selection of four beach profiles limited to the eastern part of the municipality (Figure 5.3):

1) Sandskogen, eroding profile where beach nourishment has been performed. Uncertainties concerning the sand availability, discussed in more detail in section 5.1.3.
2) Hagestad W, heavily eroding profile.
3) Hagestad E, long-term stable profile.
4) Sandhammaren, accumulating profile.

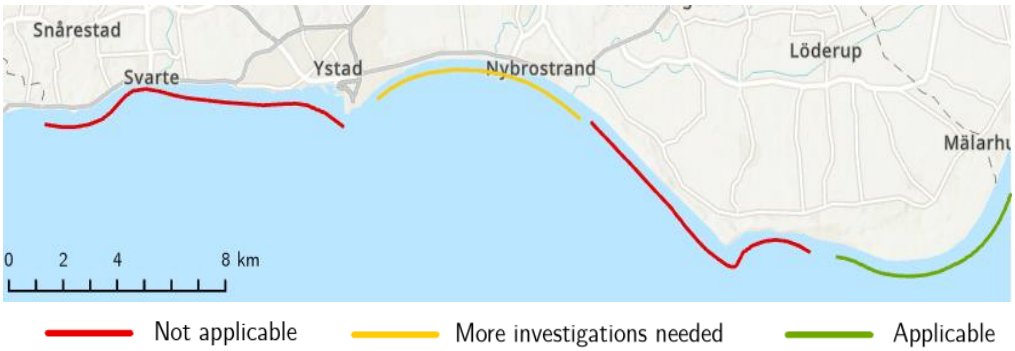

Figure 5.1: Areas where the Bruun Rule is applicable based on surface material within the active profile. The green line shows where Bruun is applicable, the orange where more investigations are required and the red line where the surface material within the profile consists of other than sand.

Figure 5.2: Historic shoreline change in Ystad municipality between 1960 – 2012 from Fredriksson et al. *(2017). Areas where the Bruun Rule is applicable in its strict form are indicated with black arrows.*

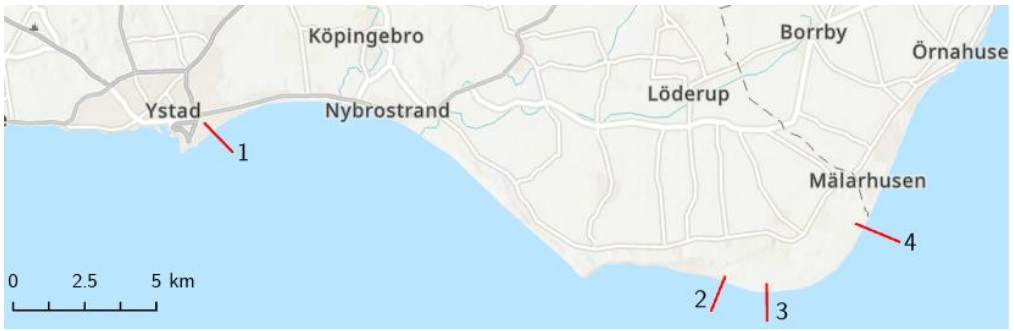

Figure 5.3 - Transects for further investigation. The first transect is located at Ystad Sandskog, where beach nourishment has been performed referred to as Sandskogen. The second transect, Hagestad W is located east of Löderups Strandbad and heavily eroding. Transect 3, Hagestad E, is long term stable. The last transect, number 4 is located at Sandhammaren and is in an accreting state.

A summary of the estimated and calculated input values for the shoreline recession models are presented in Table 5.1. The profile width is calculated using Equation (4.2). However, the calculated width differs significantly from the measured width, which is presented and discussed in section 5.1.3. The wave climate (Figure A.1) used to calculate the DoC, is based on a wave hindcast model (Adell *et al.*, 2021).

Table 5.1: Summary of input data for the four transects.

	1) Sandskogen	2) Hagestad W	3) Hagestad E	4) Sandhammaren
Grain size (mm)	0.393	0.280	0.262	0.226
Effective significant wave height (m)	2.69	3.14	2.09	2.77
Effective peak wave period (s)	11.08	10.83	10.83	10.60
Depth of closure (m)	5.73	6.58	6.12	5.85
Profile width* (m)	234	436	426	475
Beach width (m)	29.4	7.5	18.5	41.3
Berm height (m)	0.95	1.45	1.35	1.43
Dune height (m)	3.4	3.0	5.3	3.5
Shoreline change from LST gradients (m/yr)	-0.28	-3.25	0.06	3.51
Nourishment volumes (m^3/m)	279	0	0	0

* Calculated from grain size according to Equation (4.2).

5.1.2 Wave Climate

The large variation in wave height, seen in the wave record example (Figure 5.4, blue), leads to the active profile constantly adapting to new hydrodynamic forcing conditions, gradually reaching for a new equilibrium. Furthermore, seen to the seasonal variations over a year (Figure 5.4, orange), summer wave conditions are generally milder than winter wave conditions. These observations visualise the importance of investigating the equilibrium profile as an average profile over time rather than a profile measured at one point in time. In this study, the grain size data is the result from sediment samples taken at one point in time and can be suspected not to capture the effect on the beach sediment from the large variation in wave climate and forcing conditions. However, the grain size in the Bascom point is considered to be relatively unchanged over time. Still, repeated grain size sampling over time would generate a median grain size more representative for the long-term variation in forcing conditions and probably reflect the average equilibrium profile better.

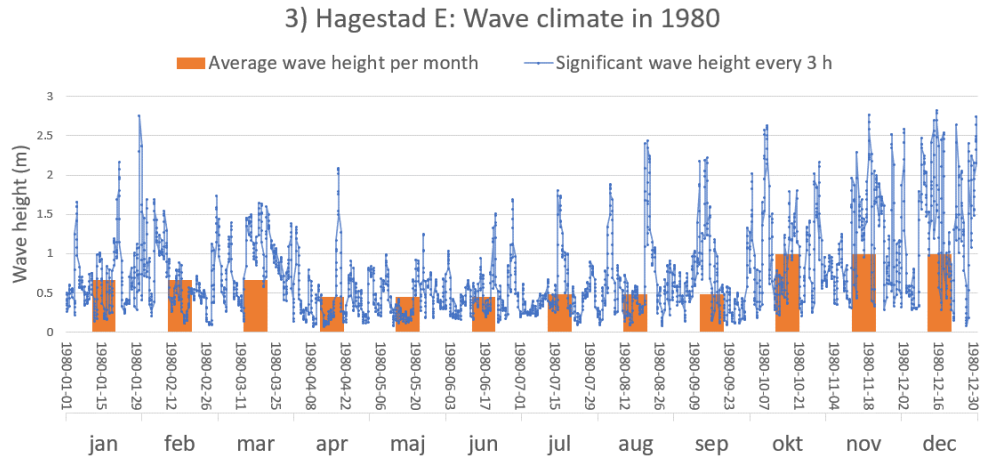

Figure 5.4: An example of wave climate visualised as significant wave height every three hours (blue) and the mean wave height (orange) every month over the year 1980 at transect Hagestad E.

5.1.3 Profile Width

Comparing the width of the equated Dean profiles calculated from median grain size with the measurements from nautical charts and low-resolution bathymetry results in a poor agreement (Table 5.2). The Dean profile is shorter than the measured width for all four transects, but the most significant deviation occurs at Sandskogen.

Table 5.2: Measured width from shoreline to DoC from nautical charts and bathymetry (115x115m) compared to the Dean profile width using grain size.

	1) Sandskogen	2) Hagestad W	3) Hagestad E	4) Sandhammaren
Nautical Chart	1100 – 1850 m	650 – 900 m	530 – 680 m	510 – 700 m
EmodNET	550 – 750 m	560 – 900 m	580 – 700 m	640 – 790 m
Equated	233 m	440 m	425 m	478 m

The profile records from repeated measurements by Hanson (2014) were only available at Sandskogen, and only to a depth of 4.5 m, which is shallower than the calculated DoC (5.7 m) for this profile. However, calculating the Dean profile width to a depth of 4.5 m results in a width of 161 m, which is almost half the width obtained from the profile records at the same depth (300 m).

The overall deviation between measured and calculated width indicates that the profiles might not be in equilibrium. However, the deviation can also be explained by a combination of several factors. Firstly, sampling grain sizes in the Bascom point might overestimate the median grain size at non-tidal beaches, resulting in a narrower calculated profile. In addition, the Bascom point sample has no information regarding the cross-shore variation in grain size distribution. Secondly, the low resolution of the bathymetry data generates large uncertainty intervals. Thirdly, nautical charts often show a shallower depth compared to reality to avoid ships running aground, thus, a wider profile is measured compared to reality. Lastly, the DoC calculated from wave data might be too shallow, contributing to a narrower profile. Access to bathymetry data with higher resolution and profile measurements performed over time would reduce the uncertainties introduced in shoreline recession

calculations and facilitate the determination of whether the profiles are in equilibrium or not.

At Knäbäckshusen, where high-resolution bathymetry data was accessible, the measured profile width also differs from the calculated Dean profile width (from a d_{50} of 0.29 mm) (Figure 5.5), around 600 m and 426 m, respectively. Except for two longshore bars, the average shape of the profile shows a resemblance to the form of an equilibrium profile. In addition, considering that the median grain size might be slightly overestimated, equating the beach profile with a smaller median grain size of 0.22 mm gives a better correlation between the measured and the Dean profile width. Varying the grain size only 0.07 mm for this profile gives a difference in profile width just over 150 m, showing that the grain size parameter is sensitive to relatively small changes. Additionally, the Dean profile repeatedly estimates shorter profiles than the observed profiles. This leads to the conclusion that basing the profile width solely on a sand sample does not provide accurate representation in many cases. Since both grain size distribution and the profile shape are dependent on the hydrodynamic forcing conditions, a sediment sample and a bathymetry observation made at the same time might have had corresponded more accurately.

The deviations between the width of the measured profiles and the Dean profiles at Hagestad W, Hagestad E and Sandhammaren could be explained by the reasons mentioned above, supported by the results from Knäbäckshusen, but to conclude whether the profiles are in equilibrium or not more detailed data and measurements are needed. However, the large deviation between the measured width and the Dean profile width at Sandskogen can not only be explained by previously mentioned reasons. For example, the non-native material from the beach nourishment probably caused an even coarser measured median grain size than what is representative, resulting in a steeper and shorter calculated profile. In addition, the profile shape is probably affected, both morphology- and transport-wise, by its proximity to Ystad Harbour and the groyne system, and elements of moraine present at the outer part of the profile (Figure 3.2), implying a non-equilibrium profile. Consequently, the Bruun Rule is not applicable here, and the Dean profile is not suitable for estimating the profile width at this location. However, model

results from Sandskogen will be included in the following sections for discussion purposes.

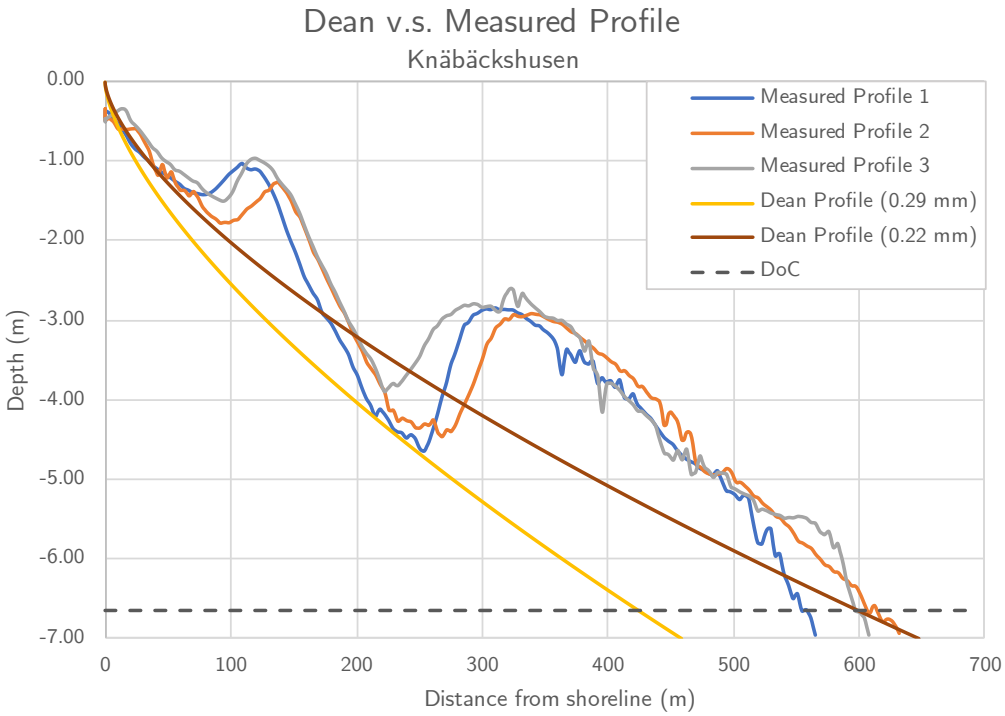

Figure 5.5: Measured and equated beach profile at Knäbäckshusen. The x-axis shows the offshore distance from the shoreline and the y-axis represents the depth. Since coordinates for the sampling location were available, three profiles were measured from bathymetry data at Knäbäckshusen 900 m apart.

5.2 The Bruun Rule

The calculated shoreline recession induced by SLR varies between the transects when applying the Bruun Rule, using input values in Table 5.1. Sandhammaren, the widest profile, will be subjected to the largest recession (-37 m to -104 m depending on RCP) and Sandskogen, the narrowest profile, will experience the least recession (-20 m to -57 m) (Table 5.3). However, considering that Sandskogen probably is not in equilibrium (discussed in section 5.1.3), the actual recession from SLR may not follow the Bruun Rule, which places additional uncertainties on the calculated recession. The results in Table 5.3 also indicate that the shore width has a negligible effect on the recession.

Table 5.3: Total recession 2150 in meters using Bruun rule in its original form and including shore width. Calculations are performed with the Dean profile width as input.

		1) Sandskogen	2) Hagestad W	3) Hagestad E	4) Sandhammaren
RCP2.6	Original	-20 m	-30 m	-32 m	-37 m
	Shore width	-22 m	-31 m	-33 m	-40 m
RCP8.5	Original	-51 m	-80 m	-84 m	-96 m
	Shore width	-57 m	-82 m	-88 m	-104 m

The recession also differs depending on climate scenario. The lower emission scenario (RCP2.6) will result in a smaller recession compared to the higher scenario (RCP8.5) for all four transects, which is expected (Figure 5.6). The time-dependent Bruun Rule shows a slightly decreasing recession rate when RCP2.6 is used, while RCP8.5 will generate an accelerated recession over time.

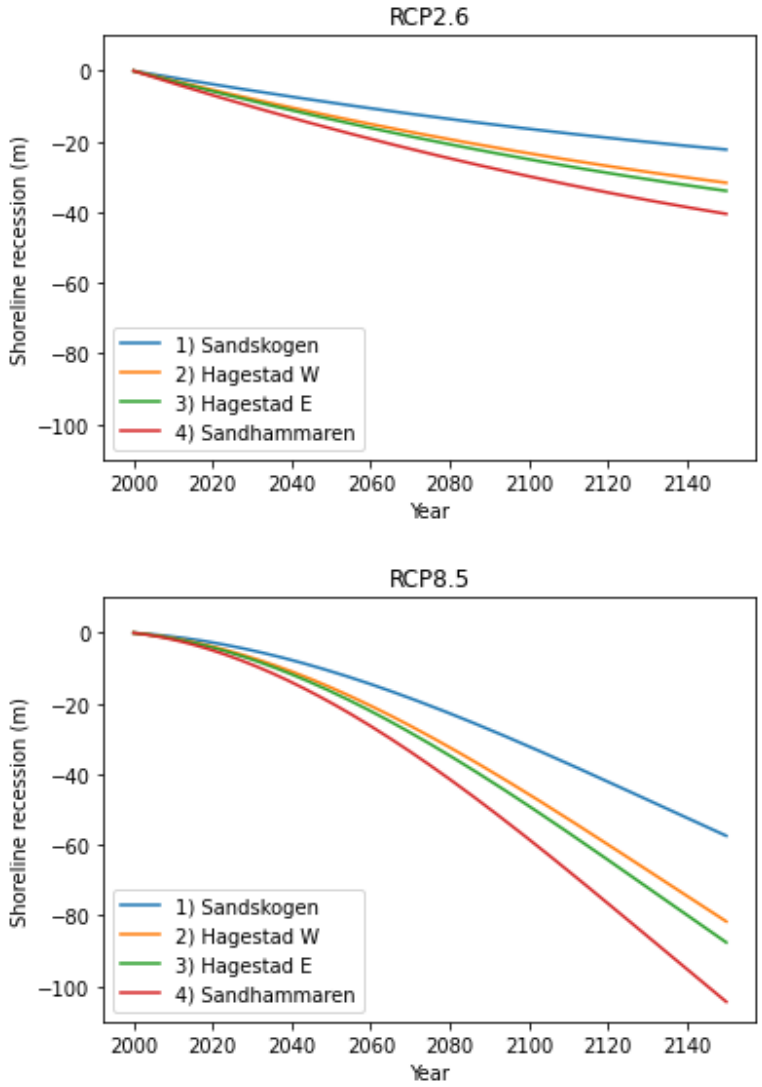

Figure 5.6: Shoreline recession 2000 - 2150 for the four profiles with scenario RCP2.6 and RCP8.5 using the Bruun rule.

5.2.1 Sensitivity Analysis

The median grain size *(d_{50})*, used to calculate the width of the subaqueous profile, and SLR *(S)* are the two parameters that, if changed, will affect the recession the most (Figure 5.7). Within the range tested in Figure 5.7a, a decrease of the grain size *(d_{50})* leads to a substantial increase in shoreline recession, since a smaller grain size leads to longer calculated subaqueous profiles, amplifying the effects of SLR. Increasing the grain size does, however, not have the same significant effect on the calculated recession. In contrast, in Figure 5.7b, both an increase and decrease of the grain size have a substantial impact on the shoreline recession. This is due to limitations in validity ranges of Equation (4.4), creating a breaking point within the tested range where the equation used to calculate the subaqueous profile length changes. The contribution from SLR is related to the mathematical linear dependence in Equation (4.6). The tested variation in the berm height *(B)* and beach width *(W_B)* have a negligible impact on the recession.

The sensitivity analysis indicates which parameters are more critical to estimate when applying the Bruun Rule, and that the relative importance of grain size can be expected to increase as the absolute value of the grain size decreases, especially for $d_{50} < 0.395$ mm. However, the parameters can be estimated with different precision, and thus this sensitivity analysis (Figure 5.7) can only describe the mathematical sensitivity of the model. Also, the sensitivity analysis is range specific and thus cannot be generalised.

The effect of the variations in estimated profile width, presented in Section 5.1.3, give rise to significant differences in Bruunian recession (Table 5.4). The largest difference in results was 357 m in Sandskogen, and in the remaining three transects, the difference was between 54 – 84 m, the longest in Hagestad W. This shows the importance of improving the method for calculating the profile width.

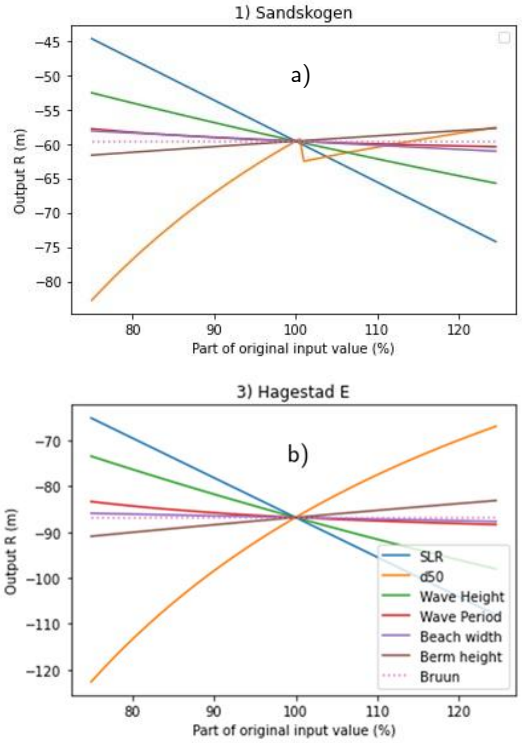

Figure 5.7: Variation in calculated recession using the Bruun Rule and varying the input parameter $\pm$ 25% in Table 5.1, one at a time. The grain size range of Sandskogen (a) overlaps the limit between two validity intervals. The general appearance of transect Hagestad E (b) corresponds well to Hagestad W and Sandhammaren, except for the magnitude of the shoreline recession.

Table 5.4: Calculated shoreline recession using the width of the Dean profile and longest measured width, respectively. The SLR-scenario used is RCP8.5

	1) Sandskogen	2) Hagestad W	3) Hagestad E	4) Sandhammaren
Dean profile	57 m	82 m	88 m	104 m
Longest measured profile	414 m	166 m	141 m	168 m
Difference	357 m	84 m	54 m	64 m

5.3 Dune Models and Edelman II

In general, including the dune system in the analysis results in a lower shoreline recession than the Bruun Rule, as seen in Figure 5.8. The difference in calculated recession between the Dune Models and the Bruun Rule is around 14 – 29 m at 1.5 m SLR, depending on transect. Hagestad W has the lowest difference, while Hagestad E has the largest difference, explained by it being the profile with the highest dune elevation, thus contributing with the largest additional sediment volume.

Some continuity can be observed in which of the Dune Models and Edelman II that generate the largest or least shoreline recession (Figure 5.8). For all profiles, the Edelman II model (orange line) gives a longer recession than the Dune Model – Basic (grey line), while the Dune Model – Topography (yellow line) is more uneven in giving more or less recession than the other models.

How large the deviation is between model output differs for each transect, seen in Figure 5.8. In Sandskogen, the relatively large variation between the models might be due to it having the shortest of the subaqueous profiles, thus the variation in dune representation plays a larger relative role in the result. At Hagestad E, the models predicted a very uniform shoreline recession. This may be because the dune shape is similar to a rectangle if excluding the small "spikes" (Figure 5.11, blue line), corresponding well to the simplified dune shape in Edelman II and Dune Model – Basic.

The Dune Model - Usable Sand (Figure 5.8, green line) was only applied at Hagestad W since it was developed to fit the dune topography of this transect (technically, it can also be applied on the other transects in a simplified way). However, the model is not applicable past the SLR of 0.5 m since the relative dune height becomes less than 0.

The assumption that the dunes will not migrate inland during SLR is not in accordance with the observations described in section 2.3.3. However, since the dunes in Hagestad W and E are steep and aeolian transport is obstructed by steep angles, the dunes in that area can be assumed not to experience any build-up. In addition, the dunes at all four transects are more or less covered

with vegetation, reducing the inland aeolian transport and probably stabilising the dunes' positions.

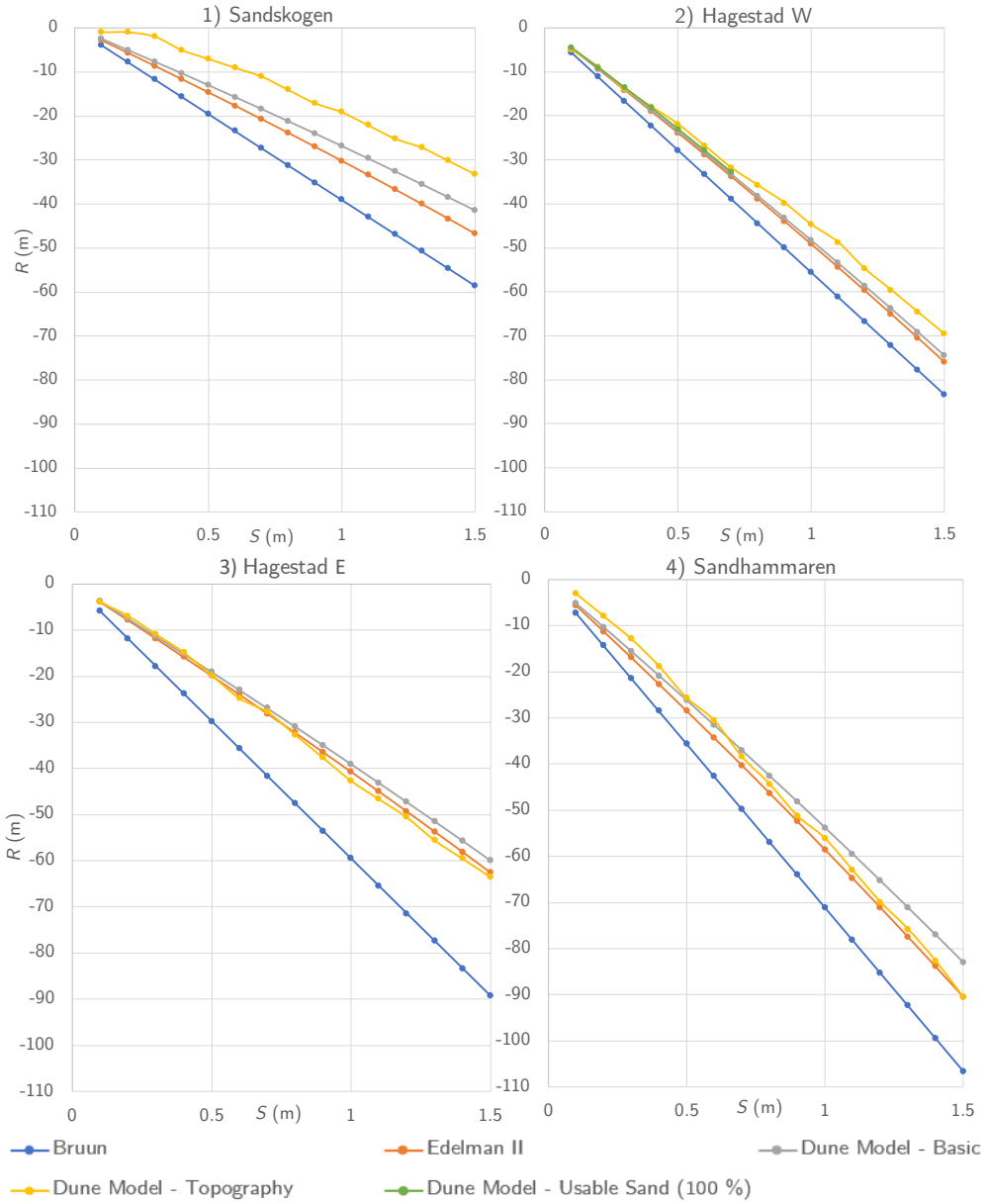

Figure 5.8: Comparison between the different Dune Models, plotted over increasing SLR.

5.3.1 Edelman II

The Edelman II model gave a lower shoreline recession than the Bruun Rule for all transects (Figure 5.8). However, looking at Figure 5.9, where the dune height of an arbitrary profile is low, Edelman II shows a marginal difference in the obtained shoreline recession, indicating there is a dune height – dune foot relationship where the Bruun Rule and the Edelman II model give the same result. The Bruun Rule decreases at a slightly slower rate than the Edelman II curve, seen in Figure 5.9, since the profile slope of the Bruun Rule is constant over time, but the profile slope in Edelman II decreases with time due to the decrease in relative dune height, and a lower slope leads to a higher recession.

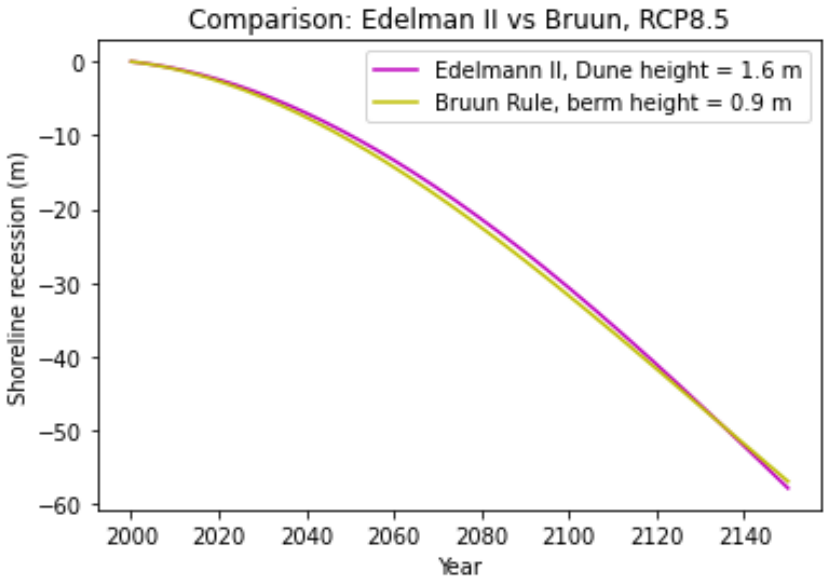

Figure 5.9: Comparison between the equations of the Edelman II model and the Bruun Rule. When a low dune height is used, the Edelman II model and the Bruun Rule give the same shoreline recession.

5.3.2 Dune Model – Basic

It can be noted in Figure 5.10 that the profiles are alike in shape but differ in dimension, e.g., the dune in Sandskogen (Figure 5.10a) is higher than the dune in Hagestad E (Figure 5.10b). In the same figures, it can also be seen that the relative dune height after SLR is lowered as in the Edelman II model, which also makes this model increase the rate of shoreline recession faster than the Bruun Rule over time. The reason why the Dune Model – Basic gives a shorter shoreline recession than the Edelman II model is much due to the non-existing beach plane in the Dune Model – Basic. For profiles with wide beaches, such as Sandskogen and Sandhammaren this gives the largest difference between these two models.

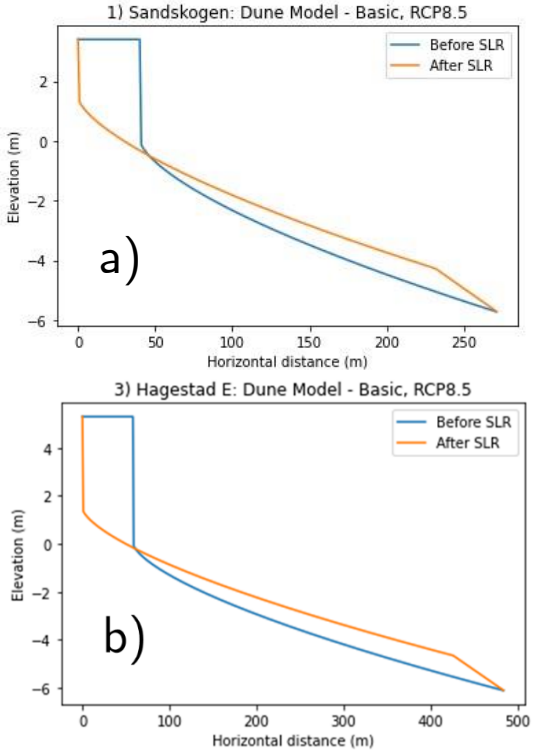

Figure 5.10: Graph showing the profile evolution of Dune Model – Basic for Sandskogen, a) for Sandskogen and b) for Hagestad E. The calculated shoreline recession is 40 m in Sandskogen and 58 m in Hagestad E, for RCP8.5. y = 0 corresponds to the mean sea level year 2000.

5.3.3 Dune Model – Topography

The Dune Model – Topography (Figure 5.8, yellow line) shows some irregularities in shoreline recession rate (Figure 5.11) due to irregularity in topography where a peak in topography leads to a lower recession rate. An example is at Sandhammaren, where the second peak to be eroded (Figure 5.11d), after the first big elevation dip at a horizontal distance of around 130 m, can be seen for Sandhammaren (Figure 5.8) between the SLR of 0.9 m – 1 m, as the sudden decrease in recession rate. Again, in the transect Sandhammaren, there is a sharp vertical line at the erosion front (Figure 5.11d). This is since the modelled landwards movement of the profile cannot yet detect dips in elevation and, in a natural way account for these dips.

The model results of Dune Model - Topography also varies with respect to giving more or less recession than the other Dune Models, much based on where the original dune top was defined and the topography inland from this point. In Sandskogen and Hagestad W, the Dune Model – Topography gives shorter shoreline recession than all the other models (Figure 5.8). This might be because the elevation increases inland from the original dune top (Figure 5.11a,b) while changes in inland topography are not accounted for in the other models. In contrast longer shoreline recession compared to Edelman is observed at the transects in Hagestad E and Sandhammaren where the dune top is higher than the nearby inland topography (Figure 5.11c,d).

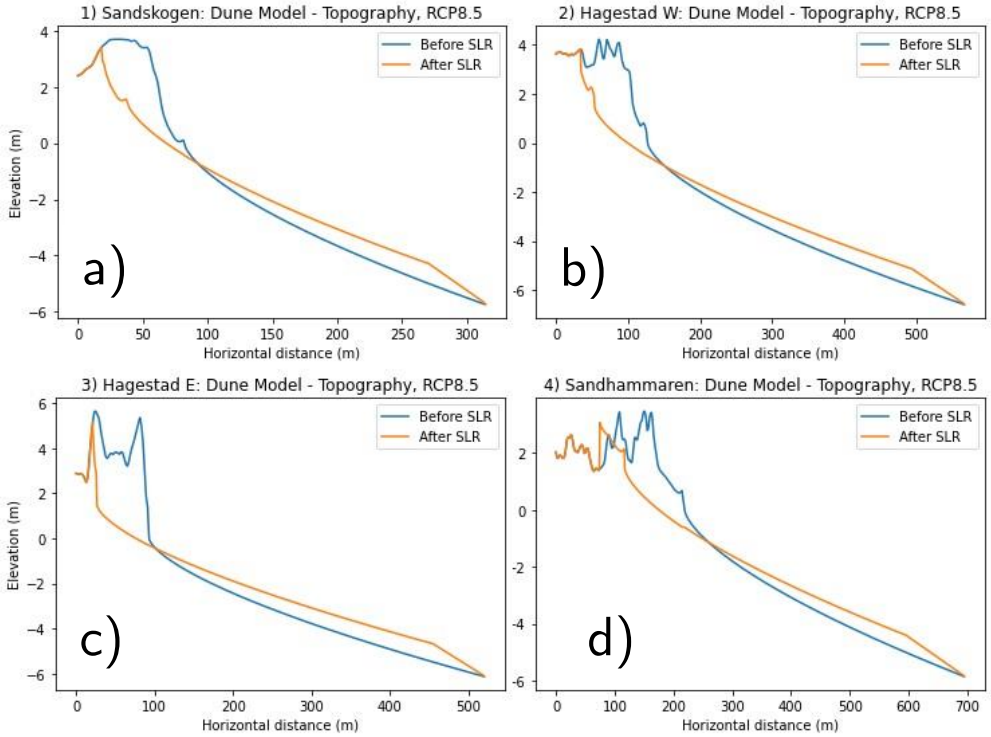

Figure 5.11: Graph showing the profile before (blue) and after (orange) SLR of the Dune Model – Topography for the transects. The climate scenario is RCP8.5. y = 0 corresponds to the mean sea level year 2000

5.3.4 Dune Model – Usable Sand

No considerable difference in results was obtained by using the usable sand coefficient (Figure 5.12). Using a coefficient value of 0 compared to 1 only gave roughly 7 m difference in shoreline recession. This might be since the dune dimensions used in the model were relatively small (Figure A.2), compared to larger dunes where the topography inland plays a more prominent role in shoreline recession, and thus also the fraction of usable sediment. Using a coefficient value of 0 gives the same recession (+1 m) as the original Bruun Rule since the dune's contribution to reducing the shoreline recession is eliminated. The small difference may be due to the small trailing ramp at the end of the profile in Dune Model – Usable sand (Figure 4.6, right side part of a_{24}). The low scenario RCP2.6 was used since the Dune Model – Usable Sand is not compatible with higher SLR with the used dune morphology.

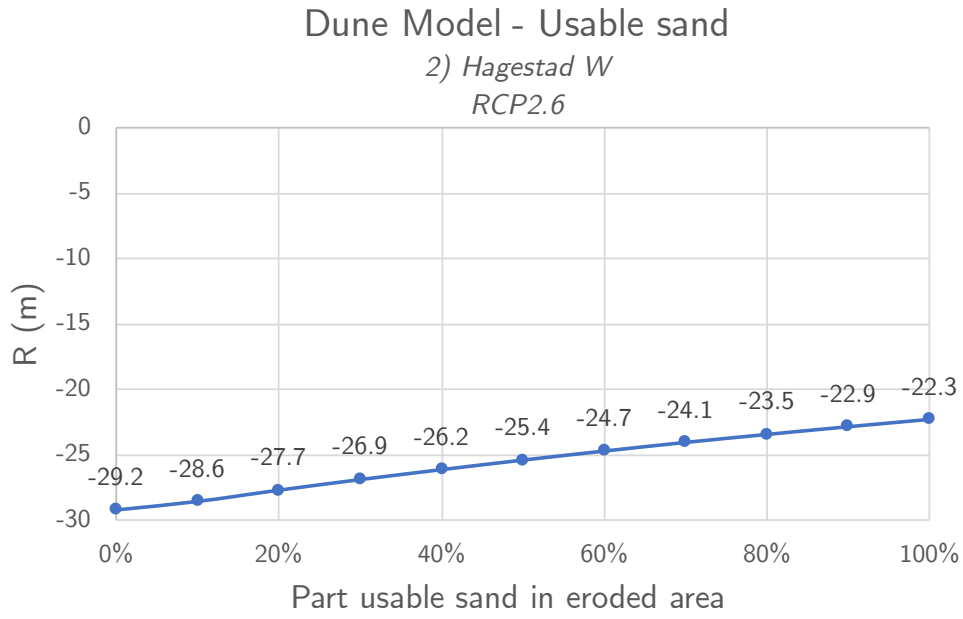

Figure 5.12: Graph showing shoreline recession as a function of the "usable sand coefficient" used in Dune model 2.0, used with the values of the second transect.

5.4 The Dean Houston Model

Including the gradients in LST, i.e., the underlying erosion or accretion, gave a significant deviation in shoreline change between the different transects (Figure 5.13). At Sandskogen, the SLR-induced recession is in the same order of magnitude as the recession caused by the gradient in LST. On the contrary, the future shoreline recession at Hagestad W is highly dominated by the LST gradient, and the SLR will play a minor role (-486 m vs -81 m). The erosion from SLR at Sandhammaren will, on the other hand, be largely compensated for by the accumulative LST gradient. At Hagestad E, which is long-term stable, the recession will increase in the future due to SLR.

The gradients in LST are estimated from overall vegetation line change for 52 years; thus, the gradients could also have captured cross-shore removal due to storms. Some processes other than LST will probably also have an effect on the vegetation line, however, the LST is assumed to be the most prominent process affecting the vegetation line. In addition, erosion of the beach plane and vegetation line might not always occur simultaneously. Furthermore, the LST is sensitive to changes in the incoming waves and angle of approach, making the assumption of a constant rate of LST gradient questionable. The impact of a future variation in LST gradients needs to be further investigated.

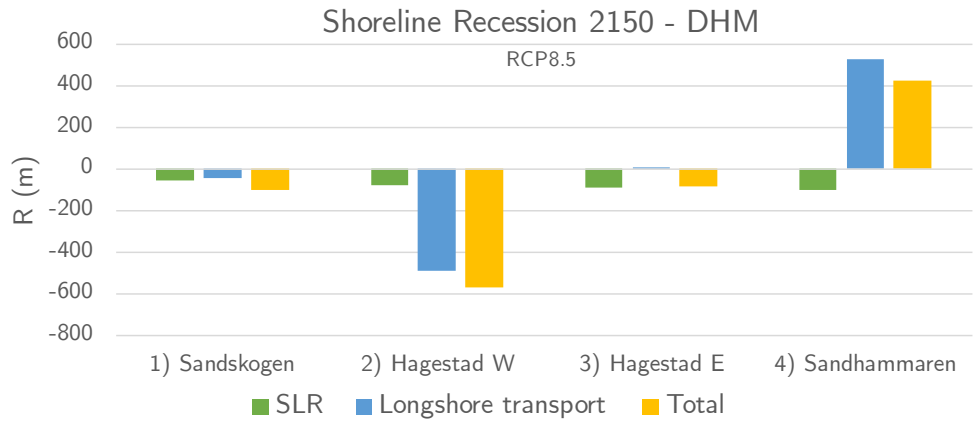

Figure 5.13: The green bar represents the recession due to SLR, the blue bar change in the shoreline's position due to longshore transport and the yellow the total change.

5.5 Beach Nourishment and Groynes

The effect from the performed beach nourishments at Sandskogen was investigated both with the DHM and the longshore spread equations.

When including the effect from beach nourishment performed at Sandskogen in the DHM, using volumes presented in Table 3.1, the total recession was reduced from 100 m to 60 m in 2150. Figure 5.14 indicates that the beach nourishment will counteract the recession, with a magnitude approximately the same as the recession caused by the LST gradient. However, this is not the case, since the DHM assumes that the added material stays within the profile for the entire period when in reality, the material will spread in the longshore direction, and the effect will be reduced, which is discussed below.

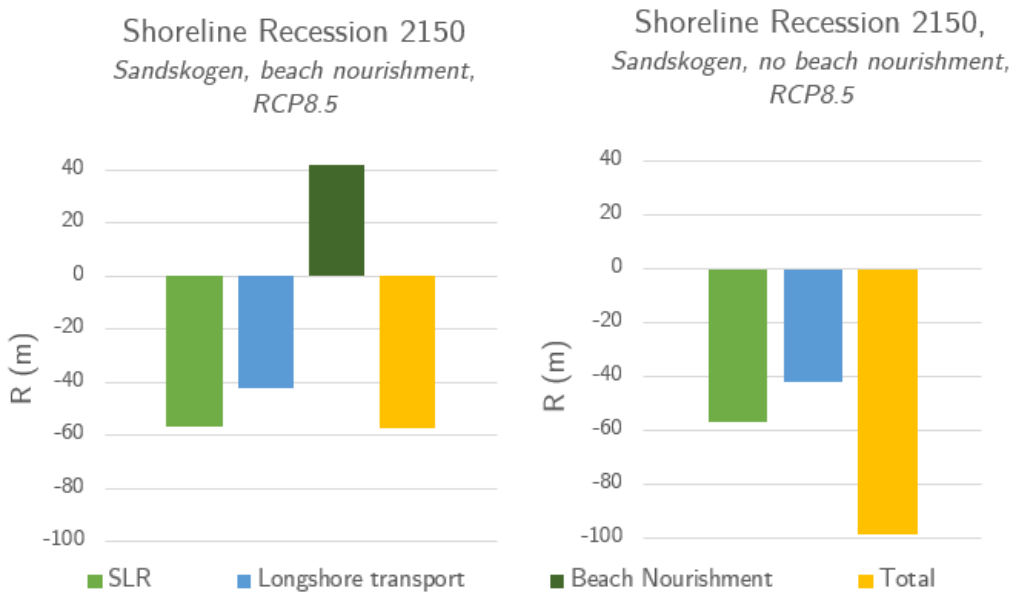

Figure 5.14: Shoreline recession at Sandskogen including SLR, LST and beach nourishment (left) and SLR and LST (right)

The two different longshore spread-equations gave similar development of the shoreline over time, and only the equation assuming a rectangular beach nourishment is presented. However, the rectangular beach nourishment has a slower spread rate, meaning the accumulative effect on the beach will last longer. Including the Bruunian recession (assuming the sediment budget is balanced) in the shoreline's development shows how the beach nourishment delays the Bruunian erosion (Figure 5.15). However, the beach nourishment effect diminishes with time. The presence of a groyne will have an accumulative effect on the shoreline updrift until the accumulation reaches the length of the groyne (in this case, 100 m), and then the sand will drift past the groyne, as can be seen in Figure 5.16. The groyne is measured to be 80 m away from the transect.

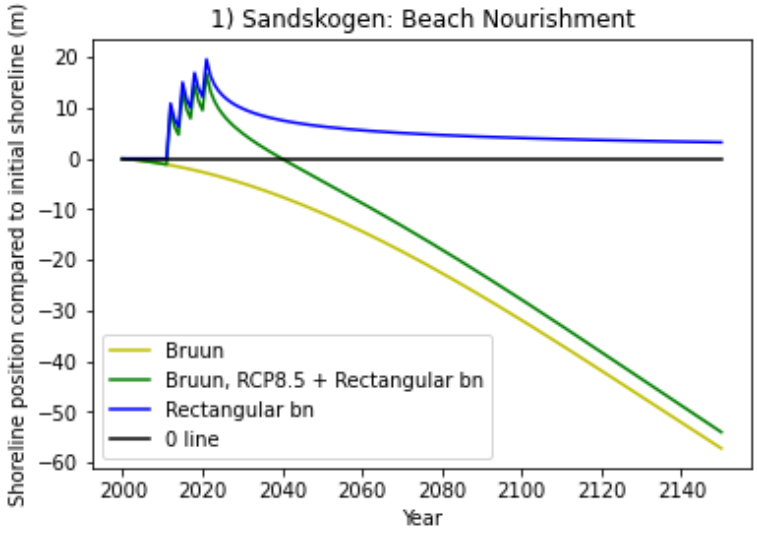

Figure 5.15: A combination of longshore spread of beach nourishment and the Bruun Rule shoreline recession is seen as the green line. The compounds are seen as the blue line: Longshore spread of a rectangular beach nourishment and the yellow line: Shoreline recession due to SLR.

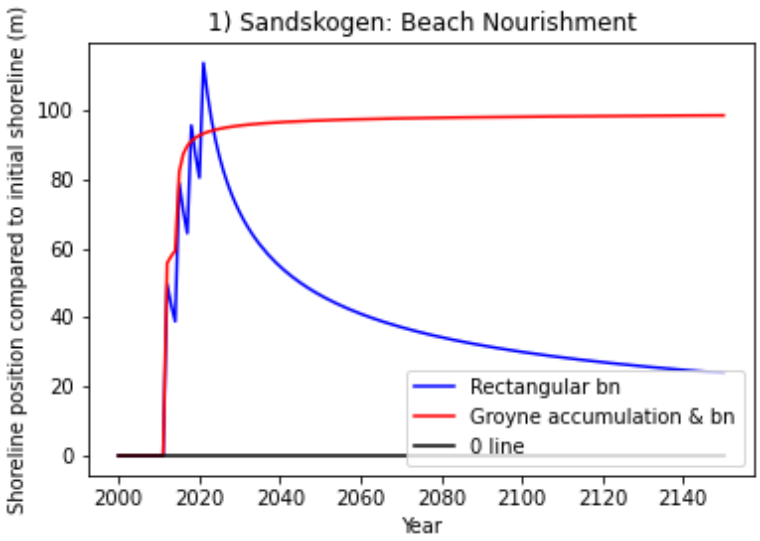

Figure 5.16: The evolution over time of the accumulation updrift a groyne (red line) compared to that of a rectangular beach nourishment (blue line). The graph shows Shoreline position over time and the data used corresponds to Transect 1.

The entire added sediment volume from the beach nourishment will not remain within the transect until 2150. Thus, in this case the DHM can be suspected to overpredict the counteraction from performed beach nourishment on the total shoreline recession in 2150. The beach nourishment will, however, reduce the retreat of the coastline, but the longshore spread should be included in the DHM for a more accurate calculation of shoreline recession. An approach could be to introduce a spread factor in the beach nourishment-term combined with more studies of the nature of the longshore spread.

5.6 Comparison of the Models

The six different models generate a recession in the same order of magnitude within each transect, except for DHM (Figure 5.17). The recession calculated with DHM highly depends on the underlying erosion/accretion, i.e., LST-gradients. At Hagestad E, which experience no long-term erosion, the DHM gave a similar recession as the five other models, while at Hagestad W, which has a severe long-term erosion, the DHM gave a recession around seven times larger compared to the other models.

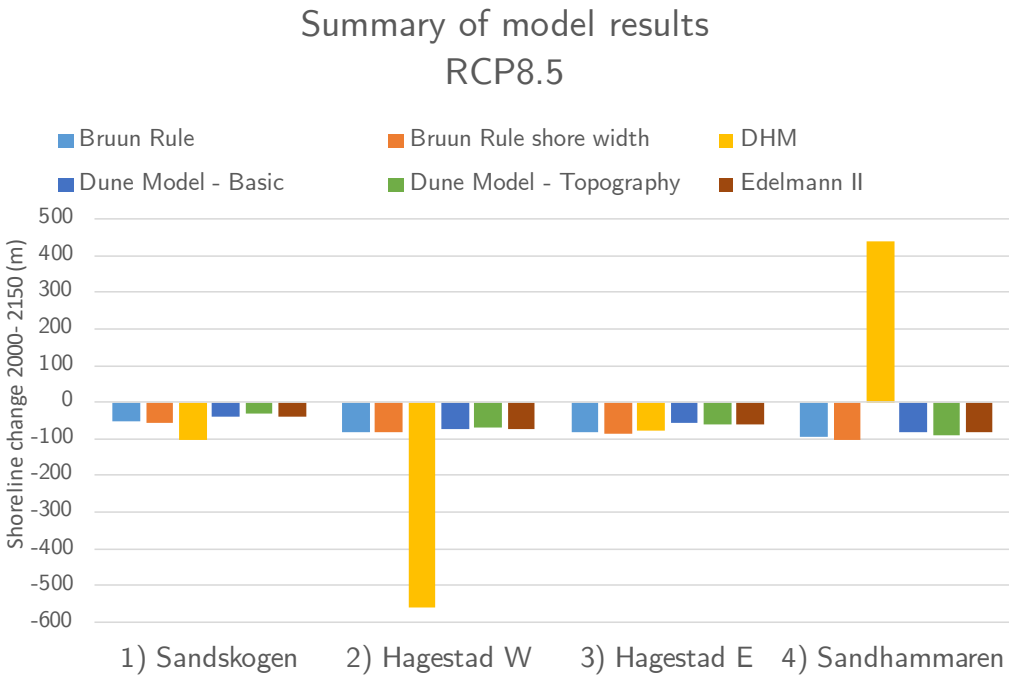

Figure 5.17: Summary of the calculated shoreline change for each model and profile.

In general, including the dune system in the calculations results in a lower recession than the Bruun Rule, but still within the same magnitude. The largest difference between the Bruun Rule and Dune Models was obtained at Hagestad E, with the highest dunes and a profile width similar to Hagestad W and Sandhammaren. Therefore, it can be concluded that the larger the dune elevation is, the more the recession is reduced. In addition, at Sandskogen, a

difference between the Bruun Rule and Dune Models is also visible. The dune elevation is similar to Hagestad W and Sandhammaren, but the profile width is shorter; hence, with a shorter profile, lower dunes can still reduce the recession.

The models used to develop the Bruun Rule as concerning only the SLR, including more of the beach, showed varying results. What model is the best is difficult to say since not much data is available, and in nature, many other factors matter.

5.7 Monte Carlo Simulation

The results presented in previous sections are deterministic, which provides one single value for future shoreline recession for each transect and model setup. But shoreline recession cannot be calculated with the level of accuracy indicated previously in this chapter, as there are uncertainties related to the parameters used in the calculations. Nevertheless, a deterministic approach was seen as suitable in this study, given the aim of this thesis; to compare different Bruun Rule-based models for estimating future shoreline recession. A more accurate way of illustrating possible future outcomes to use in coastal management would be a probabilistic approach, e.g., with a Monte Carlo simulation. In the probabilistic approach, all parameters are assigned probability distributions and intervals instead of unique values. It falls outside the scope of this study to take a full probabilistic approach. As a way of illustrating the importance of adopting a probabilistic view on future shoreline recession in future research and applications, an example of what type of results a probabilistic approach would generate is presented. The probability distributions and intervals are assumed to be reasonable based on available data, but further research is needed to determine both the true distributions and more accurate intervals.

The MC-simulation performed with the Bruun Rule, only including SLR-induced recession, resulted in a wide range of possible outcomes, up to 90 m difference within each profile (Figure 5.18). The wide ranges result from the uncertainty in the input data. Even though the calculated recession presented in section 5.2 falls within the most probable part of the intervals, there is still

a large likelihood that the actual recession will significantly deviate from those values. Therefore, using the deterministic approach is not recommended to use in coastal planning and management but instead use a probabilistic approach.

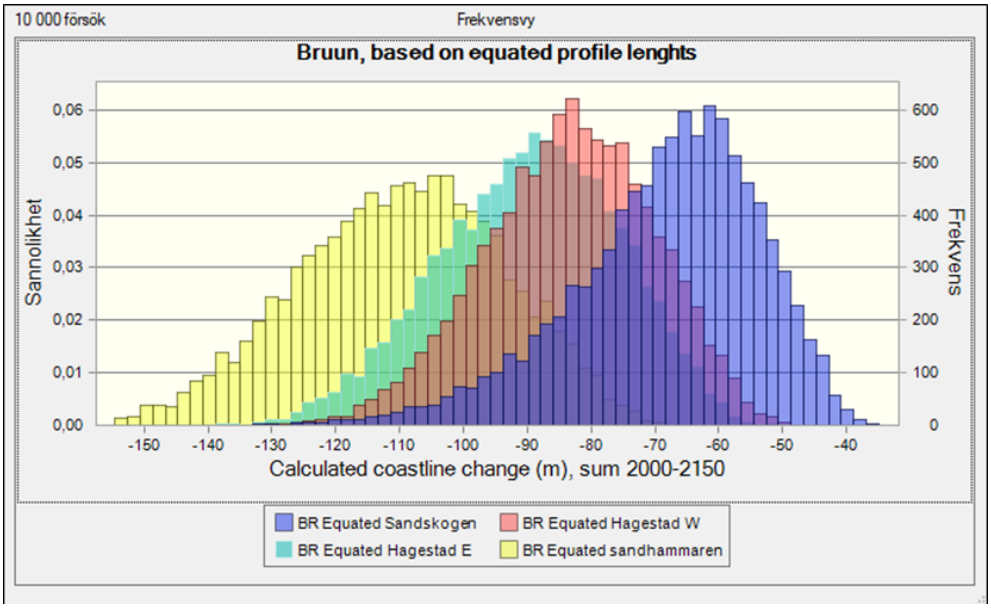

Figure 5.18: Calculated probability intervals for SLR-induced shoreline recession for RCP8.5. The left y-axis corresponds to the probability.

The magnitude of recession changes significantly when including the underlying erosion and LST-gradients in the MC simulation, depending on profile (Figure 5.19). Similar to the results in section 5.4, Sandhammaren, with the largest recession using only the Bruun Rule now experiences accumulation instead, while Hagestad W will retreat the most. In addition, the ranges of recession for all profiles are around 100 m wider compared to the ranges in Figure 5.18, which originates from the effect of LST-gradients. However, the probability interval of the LST-gradient was not thoroughly investigated since this was outside the scope of this thesis. Still, given the significant difference in shoreline recession, the underlying erosion from LST-gradients is important to include in predictions, and the variation and probability distribution of the intervals should be better assessed.

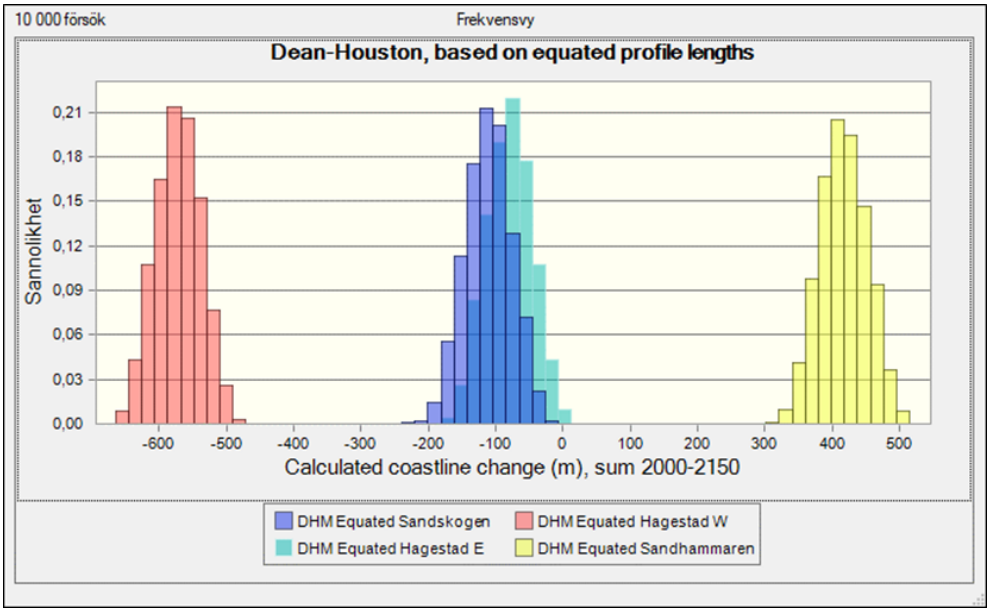

Figure 5.19: Probability intervals for the shoreline recession using the DHM and RCP8.5. The y-axis corresponds to the probability.

The MC-run where different probability distributions were assigned to the two most sensitive parameters, SLR *(S)* and the scale parameter *(A)*, showed that, in this case, the type of distribution assigned is not the main factor affecting the resulting recession interval, but rather the range of input values. In Figure 5.20, the turquoise bar chart has the same distributions and intervals as presented above, and the pink bar chart also represents a triangular distribution on S and A, but has larger assigned intervals, generating a larger recession interval. The blue and pink bar charts are the result from assigning a normal and triangular probability distribution respectively for S and A, but the minimum and maximum values are approximately the same. The resulting recession intervals have the same size, but with a more centred weight for the normal distribution. The sensitivity analysis was only performed on the transect Hagestad W since it had a symmetrical interval for the A parameter.

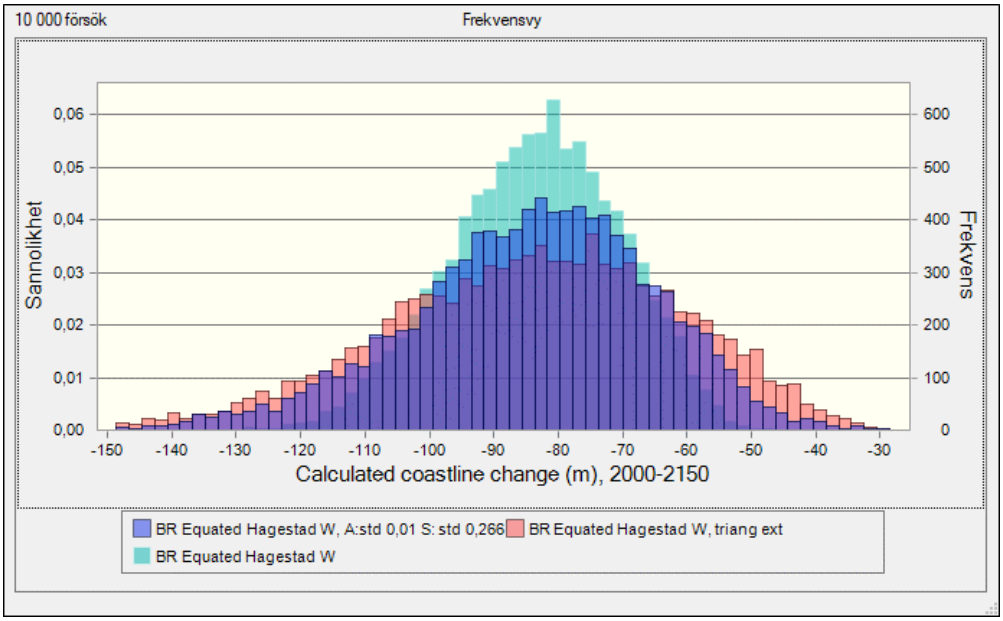

Figure 5.20: Results of the sensitivity analysis of the probability distribution, where the blue bar chart shows the result from applying a normal distribution to the two most sensitive parameters, the turquoise shows the result as presented earlier with triangular distributions and the pink graph shows a run with triangular distributions, only that the interval of SLR is set to the outmost "boundaries" of the normal distribution. The left y-axis corresponds to the probability.

The normal distribution is more likely to occur in nature than the triangular distribution and it accounts for the whole range of possible outcomes from IPCC, whereas the triangular is simplified to accounting for the likely range. The normal distribution for the A parameter is also more likely to occur than the triangular, however, there is not enough available data to estimate the actual standard deviation. On the other hand, there is not enough data to state that the interval of the triangular distribution has the strict assigned min- and max values either, but using the observed range involves less conjecture. Thus, there are pros and cons with using both probability intervals, given the low availability of data.

6 Conclusions and Recommendations

The most important conclusions from the method comparison are firstly that LST-gradients and the background erosion can highly affect the future recession and is an important factor to consider in risk assessment. Secondly, that including the dune system in the SLR-induced recession calculations generates a lower recession in Ystad municipality, however still in the same order of magnitude as using the original Bruun Rule. In addition, how much the estimated shoreline change differs between methods used is site-specific. Thus, what model that is the most suitable in a coastal management or planning project will depend on what type of features and processes that are present at the concerned section of the coast. For example, the dune system is more important to include when larger dunes are present. The LST gradients are more important to consider in future estimations for an eroding or accreting beach compared to a long-term stable beach.

In Ystad municipality, the Bruun Rule is not well suited for a large part of the coastline because of the low amount of sand in the surface material. Even in areas where the sand amount within the profile is sufficient, the assumption of the equilibrium profile concept could not be confirmed with the available data; consequently, there are questions whether the Bruun Rule and its modifications are valid or not within these areas. In order to make well based decisions in coastal management and planning, it needs to be further investigated whether the areas of interest are in equilibrium or not before estimating the shoreline change with the Bruun Rule or its developments.

Below follows a recommendation on how to improve the projections for future shoreline recession when using the Bruun Rule and its developments.

Recommendations and future research:

- Access to higher quality data is essential. Due to the dynamic nature of the nearshore area, repeated profile measurements over time are needed to cover seasonal and annual variations to detect DoC and validate the equilibrium profile assumption. Availability of high-resolution bathymetry data is also needed to determine the profile width more accurately.

- Better estimations of the LST-gradient and possible future variation. The LST is highly sensitive to the inclination angle of the incoming waves, and the future morphological changes might thus highly affect the erosion state in some areas. To be able to better account for the underlying LST rate gradients, projections for future LST needs to be investigated, including the probable interdependency with the SLR. Also, since there are various measurement methods with different limitations and advantages, this should be developed further.
- Extensive grain size measurements and accurate reference point. Within the range of values relevant for the studied area, the calculated profile width is sensitive to small changes in the grain size, thus extensive measurements, and investigations regarding the accuracy of using the Bascom point as reference point on low-tidal beaches are recommended.
- Examining the importance of including the grain size variation across the profile should be done, to gain a better understanding of how the profiles geometry and coastal response are affected by this variation.
- In a coastal response assessment, offshore sediment excess should be evaluated. In this study, the Dean transport has been neglected since the available data was not enough to determine the offshore sediment availability, however, if present, excessive offshore sand might lead to accretion of the beach instead of recession.
- When assessing the coastal response, the dune volume and sediment exchange with the beach should be investigated. Including dunes in the model could be of importance. In this study, the dunes have been assumed to not migrate inland, which might be a reasonable assumption for some dune formations. However, the beach – dune relation is not always the same. Very high or very low dunes could generally be expected to be of higher importance than medium dunes due to the excess or deficit sediment supply.
- The future shoreline position change should be presented using probability intervals rather than a fixed line on a map, given the large

uncertainties in available data and in long term modelling of complex processes. This can be done with a Monte Carlo simulation.

- On non-sandy coastlines, other more well-suited models should be used. Non-sandy coastlines materials will not respond in the same way to the forcing conditions as sandy coastlines. Thus, other models are needed to estimate the recession on these coastlines.

7 References

Adell, A. *et al.* (2021) 'Open-access portal with hindcast wave data for Skåne and Halland', *VATTEN – Journal of Water Management and Research.* 2, pp. 81-90. Available at: https://gis.swedgeo.se/vagmodell/.

Atkinson, A. L. *et al.* (2018) 'Laboratory investigation of the Bruun Rule and beach response to sea level rise', *Coastal Engineering*, 136, pp. 183–202. doi: 10.1016/j.coastaleng.2018.03.003.

Bascom, W. N. (1951) 'The realtionship between sand size and beach-face slope', *EOS - Transactions, Amercian Geophysical Union*, 32(6), pp. 866–874.

Berin, I. and Löwdin, J. (2021) *Longshore Sediment Transport Along the Coast of Ystad Municipality - Cause and Effect* [Unpublished]. Master Thesis, Dept. Water Res. Engrg, Lund University.

Bird, E. (2000) *Coastal Geomorphology: An Introduction.* 1st edn. Chichester: Wiley.

Bodge, K. R. (1992) 'Representing equilibrium beach profiles with an exponential expression', *Journal of Coastal Research*, 8(1), pp. 47–55.

Boon, J. D. and Green, M. O. (1989) 'Caribbean beach-face slopes and beach equilibrium profiles', *Proc. 21st Int. Coastal Engng. Conf.*, pp. 1618–1630. doi: 10.9753/icce.v21.120.

Borell Lövstedt, C. and Persson, O. (2015) *Kustförvaltningsplan för Ystads kommun.* Malmö: Sweco.

Bruun, P. (1954) 'Coast erosion and the development of beach profiles', *Technical Memorandum*, 44, pp. 1–27.

Bruun, P. (1962) 'Sea-Level Rise as a Cause of Shore Erosion', *Journal of Waterways and Harbors Division, ASCE*, 4, pp. 117–130.

Bruun, P. (1983) 'Review of conditions for uses of the Bruun rule of erosion', *Coastal Engineering*, 7(1), pp. 77–89. doi: 10.1016/0378-3839(83)90028-5.

Bruun, P. (1988) 'The Bruun Rule of Erosion by sea-level rise: a discussion on large- scale two- and three-dimensional usages', *Journal of Coastal Research*, 4(4), pp. 627–648.

Cooper, J. A. G. *et al.* (2020) 'Sandy beaches can survive sea-level rise', *Nature Climate Change*, 10(11), pp. 993–995. doi: 10.1038/s41558-020-00934-2.

Cooper, J. A. G. and Pilkey, O. H. (2004) 'Sea-level rise and shoreline retreat: Time to abandon the Bruun Rule', *Global and Planetary Change*, 43(3–4), pp. 157–171. doi: 10.1016/j.gloplacha.2004.07.001.

Dahlerus, C.-J. and Egermayer, D. (2005) *Uppspolning och klittererosion längs Ystadkusten - Situation idag och framtida scenarier*. Master Thesis No. 2005:11, Dept. Water Res. Engrg, Lund University. Available at: http://lup.lub.lu.se/student-papers/record/1326239.

Davidson-Arnott, R. (2005) 'Conceptual model of the effects of sea level rise on sandy coasts', *Journal of Coastal Research*, 21(6), pp. 1166–1172. doi: 10.2112/03-0051.1.

Davidson-Arnott, R. (2010) *Introduction to Coastal Processes and Geomorphology*. Cambridge: Cambridge University Press.

Davidson-Arnott, R. (2012) 'Wave-Dominated Coasts', in *Treatise on Estuarine and Coastal Science*. Elsevier Inc., pp. 73–116. doi: 10.1016/B978-0-12-374711-2.00305-3.

Dean, R. G. (1977) 'Equilibrium beach profiles: U.S. Atlantic and Gulf coasts', *Ocean Engineering Report*, Newark: Dept. Civil Engrg. (Ocean Engng Report No. 12).

Dean, R. G. (1983) 'Principles of beach nourishment', in Komar, P. D. (ed.) *CRC Handbook of coastal processes and erosion*. Boca Raton, Florida: CRC Press inc., pp. 217–231.

Dean, R. G. (1987) 'Additional sediment input to the nearshore region.', *SHORE and BEACH*, 55(3-4 , Jul.), pp. 76–81.

Dean, R. G. (1991) 'Equilibrium Beach Profiles: Characteristics and Applications', *Journal of Coastal Research*, 7(1), pp. 53–84. Available at: http://www.jstor.org/stable/4297805.

Dean, R. G. (2002) *Beach Nourishment: Theory and Practise*. 5 Toh Tuck Link, Singapore: WORLD SCIENTIFIC (Advanced Series on Ocean Engineering). doi: 10.1142/2160.

Dean, R. G. and Dalrymple, R. A. (2004) *Coastal Processes with Engineering Applications*. Cambridge: Cambridge University Press.

Dean, R. G. and Houston, J. R. (2016) 'Determining shoreline response to sea level rise', *Coastal Engineering*, 114, pp. 1–8. doi: 10.1016/j.coastaleng.2016.03.009.

Dean, R. G., Kriebel, D. L. and Walton, T. L. (1995) 'Cross-Shore Sediment Transport Processes', in *Coastal Engineering Manual*. U.S. Army Coastal & Hydraulics Laboratory, pp. 159–220. doi: 10.1142/9789812797582_0004.

Dean, R. G. and Maurmeyer, E. M. (1983) 'Models for beach profile response', in Komar, P. D. (ed.) *CRC Handbook of coastal processes and erosion*. 2nd edn, pp. 151–165.

Edelman, T. (1972) 'Dune Erosion During Storm Conditions.', *Proc. 13th Coastal Engng. Conf.*, pp. 1305–1311. doi: 10.1061/9780872620490.073.

EMODnet Bathymetry Consortium (2020) *EMODnet Digital Bathymetry (DTM)*. Available at: https://sextant.ifremer.fr/record/bb6a87dd-e579-4036-abe1-e649cea9881a/ (Accessed: 5 April 2021).

Everts, C. H. (1985) 'Sea Level Rise Effects on Shoreline Position', *Journal of Waterway, Port, Coastal, and Ocean Engineering*, 111(6), pp. 985–999.

Falqués, A. (2003) 'On the diffusivity in coastline dynamics', *Geophysical Research Letters*, 30(21), pp. 1–5. doi: 10.1029/2003GL017760.

Fenneman, N. M. (1902) 'Development of the Profile of Equilibrium of the Subaqueous Shore Terrace', *The Journal of Geology*, 10(1), pp. 1–32.

Fredriksson, C. *et al.* (2017) 'Sandbehov för att motverka stranderosion utmed Skånes sydkust under perioden 2017 – 2100', *VATTEN - Journal of Water Management and Research*, 73(November), pp. 77–84.

Gallop, S. L. *et al.* (2020) 'Geologically controlled sandy beaches: Their geomorphology, morphodynamics and classification', *Science of the Total Environment*, 731(139123). doi: 10.1016/j.scitotenv.2020.139123.

Hallermeier, R. J. (1978) 'Uses for a Calculated Limit Depth To Beach Erosion.', *Proc. 16th Coastal Engng. Conf.*, pp. 1493–1512. doi: 10.9753/icce.v16.88.

Hallin, C. (2019) Long-term beach and dune evolution - Development and application of the CS-model. Diss., Lund: Dept. Water Res. Engrg., Lund University.

Hands, E. B. (1984) The great lakes as a test model for profile response to sea level changes. Washington DC: CERC (Report No. CERC-84-14.)

Hanson, H. (2021). Personal communication (2021-03-03).

Hanson, H. (2021). Personal communication (2021-06-04).

Hanson, H. (2014) *Profilmätningar vid Ystad Sandskog och Löderups strandband*. Technical Report, Dept. Water Res. Engrg, Lund University.

Hanson, H. and Almström, B. (2013) Strandfodringen i Ystad 2011 - bakgrund, uppföljning, framtid. Malmö: Sweco.

Helland-Hansen, W. and Hampson, G. J. (2009) 'Trajectory analysis: Concepts and applications', *Basin Research*, 21(5), pp. 454–483. doi: 10.1111/j.1365-2117.2009.00425.x.

Hieronymus, M. and Kalén, O. (2020) 'Sea-level rise projections for Sweden based on the new IPCC special report: The ocean and cryosphere in a changing climate', *Ambio*, 49(10), pp. 1587–1600. doi: 10.1007/s13280-019-01313-8.

Holman, R. A. *et al.* (2014) 'A parametric model for barred equilibrium beach profiles', *Coastal Engineering*, 90, pp. 85–94. doi: 10.1016/j.coastaleng.2014.03.005.

Houston, J. R. (2015) 'Shoreline Response to Sea-Level Rise on the Southwest Coast of Florida', *Journal of Coastal Research*, 31(4), pp. 777–789. doi: 10.2112/JCOASTRES-D-14-00161.1.

IPCC, 2019: 'Technical Summary' [H.-O. Pörtner, D.C. Roberts, V. Masson-Delmotte, P. Zhai, E. Poloczanska, K. Mintenbeck, M. Tignor, A. Alegría, M. Nicolai, A. Okem, J. Petzold, B. Rama, N.M. Weyer (eds.)]. In: *IPCC Special Report on the Ocean and Cryosphere in a Changing Climate* [H.- O. Pörtner, D.C. Roberts, V. Masson-Delmotte, P. Zhai, M. Tignor, E. Poloczanska, K. Mintenbeck, A. Alegría, M. Nicolai, A. Okem, J. Petzold, B. Rama, N.M. Weyer (eds.)]. In press.

Karasu, S. *et al.* (2008) 'Coupled Longshore and Cross-Shore Models for Beach Nourishment Evolution at Laboratory Scale', *Journal of Waterway, Port, Coastal, and Ocean Engineering*, 134(1), pp. 30–39. doi: 10.1061/(asce)0733-950x(2008)134:1(30).

Karunarathna, H. *et al.* (2018) 'Multi-timescale morphological modelling of a dune-fronted sandy beach', *Coastal Engineering*, 136, pp. 161–171. doi: 10.1016/j.coastaleng.2018.03.005.

Koktas, M. (2017) *The Effect of Variable Grain Size Distribution on Beach's morphological response*. MSc Thesis, Department of Hydraullic Engineering, Delft University of Technology.

Komar, P. D. and McDougal, W. G. (1994) 'The analysis of exponential beach profiles', *Journal of Coastal Research*, 10(1), pp. 59–69.

Kraus, N. C. and Dean, J. L. (1987) 'Longshore Sediment Transport Rate Distributions Measured By Trap', in Kraus, N. C. (ed.) *Proc. Coastal Sediments '87*. New Orleans, Louisiana: ASCE, pp. 881–896.

Kriebel, D. L. and Dean, R. G. (1993) 'Convolution method for time-dependent beach-profile response', *Journal of Waterway, Port, Coastal, and Ocean Engineering*, 119(2), pp. 204–226.

Kriebel, D. L., Kraus, N. C. and Larson, M. (1991) 'Engineering methods for predicting beach profile response', in *Proc. Coastal Sediments '91 Conference*. Seattle, pp. 557–571.

Lantmäteriet (2021) *Markhöjdmodell grid +1*. Available at: https://www.geodata.se/geodataportalen/srv/swe/catalog.search;jsessionid=

EADE3B1ECF2BEEB61C3440994CCF05D5#/metadata/c510e63f-0bf3-46c9-ab8b-3b37a898af85.

Lantmäteriet (no date) *Eniro Karta*. Available at: https://kartor.eniro.se/?c=55.417615,14.022675&z=12&l=aerial (Accessed: 15 March 2021).

Larson, M. (1991) 'Equilibrium profile of a beach with varying grain size', in Kraus, N. C., Gingerish, K. J., and Kriebel, D. L. (eds) *Proc. Coastal sediments '91*. ASCE, pp. 905–918.

Larson, M., Erikson, L. and Hanson, H. (2004) 'An analytical model to predict dune erosion due to wave impact', *Coastal Engineering*, 51(8–9), pp. 675–696. doi: 10.1016/j.coastaleng.2004.07.003.

Larson, M., Hanson, H. and Kraus, N. C. (1987) *Analytical solutions of the one-line model of shoreline change*. Technical Report CERC 87 15, US Army Engineer Waterways Experiment Station, Coastal Engineering Research Center, 100 pp.

Larson, M. and Kraus, N. C. (1991) 'Mathematical modeling of the fate of beach fill', *Coastal Engineering*, 16(1), pp. 83–114. doi: 10.1016/0378-3839(91)90054-K.

Larson, M., Kraus, N. C. and Wise, R. A. (1998) 'Simple models for equilibrium profiles under breaking and non-breaking waves', *Proc. Coastal Enging. Conf.*, 3, pp. 2722–2735. doi: 10.1061/9780784404119.206.

Leatherman, S. P., Zhang, K. and Douglas, B. C. (2000) 'Sea level rise shown to drive coastal erosion', *Eos*, 81(6), pp. 55–57. doi: 10.1029/00EO00034.

Lindell, J., Fredriksson, C. and Hanson, H. (2017) 'Impact of Dune Vegetation on Wave and Wind Erosion - a Case Study at Ängelholm Beach, South Sweden', *VATTEN – Journal of Water Management and Research*, 73(January), pp. 39–48. Available at: http://www.tidskriftenvatten.se/wp-content/uploads/2017/09/39-50-Vatten-1-2-17_opt.pdf.

Malmberg-Persson, K. et al. (2016) Skånes känsliga stränder – erosionsförhållanden och geologi för samhällsplanering. Uppsala: SGU (SGU Report 2016:17)

Mcfall, B. C. (2019) 'The Relationship between Beach Grain Size and Intertidal Beach Face Slope', *Journal of Coastal Research*, 35(5), pp. 1080–1086. doi: 10.2112/JCOASTRES-D-19-00004.1.

Nerheim, S. and Johansson, L. (2018) *Extremvattenstånd i ystad*. Karlstad: SMHI.

Nerheim, S., Schöld, S. and Persson, G. (2017) 'Framtida havsnivåer i Sverige', *SMHI: Klimatologi*, (48).

Nyberg, J. *et al.* (2020) *Kustnära sedimentdynamik*. Uppsala: SGU (SGU Report 2020:04).

Ohlsson, M. (2008) Bakgrundsmaterial-Policy för förvaltning och skydd av kusten. Ystad Kommun.

Ohlsson Skoog, M. and Green, A. (2018) *Handlingsplan för förvaltning och skydd av kusten*. Ystad Kommun.

Pelnard-Considere, R. (1956) 'Essai de theorie de l'evolution des formes de rivage en plages de sable et de galets', *Les Energies de la Mer: Compte Rendu Des Quatriemes Journees de L'hydraulique*, Paris 13, 14 and 15 Juin 1956; Question III, rapport 1, 74-1-10, pp. 289–298.

Pilkey, O. H. *et al.* (1993) 'The concept of shoreface profile of equilibrium: a critical review', *Journal of Coastal Research*, 9(1), pp. 255–278.

Preoteasa, L. and Vespremeanu-stroe, A. (2010) 'Grain-Size Analysis of the Beach-Dune Sediments and the Geomorphological Significance', *Revista de Geomorfologie*, 12, pp. 73–79.

Van Rijn, L. C. (2002) 'Longshore sand transport', in *Proc. of the Coastal Engng Conference*, pp. 1–13.

Rosati, J. D. (2005) 'Concepts in sediment budgets', *Journal of Coastal Research*, 21(2), pp. 307–322. doi: 10.2112/02-475A.1.

Rosati, J. D., Dean, R. G. and Walton, T. L. (2013) 'The modified Bruun Rule extended for landward transport', *Marine Geology*, 340, pp. 71–81. doi: 10.1016/j.margeo.2013.04.018.

Sadat-Helbar, S. M. *et al.* (2009) 'Fall Velocity of Sediment Particles', in Trilling, L. et al. (eds) *4th IASME/WSEAS Int. Conference on Water Resources, Hydraulics & Hydrology*. Cambridge, UK: WSEAS Press, pp. 39–45. doi: 10.1061/9780784404003.ch03.

SCALGO Live (no date) *Scalgo Live*. Available at: https://scalgo.com/live/sweden?res=1&ll=14.117332%2C55.383393&lrs=sweden%2Fsweden%3Aortho%3A3006%3A20210219%3Ase125&tool=query (Accessed: 15 March 2021).

Schlager, W. (1993) 'Accommodation and supply-a dual control on stratigraphic sequences', *Sedimentary Geology*, 86(1–2), pp. 111–136. doi: 10.1016/0037-0738(93)90136-S.

Schmidt, E. (2016) *Nearshore Currents in Southeastern Scania*. Master Thesis No. 16/5015, Dept. of Water Res. Engrg., Lund University.

Schwartz, M. L. (1967) 'The Bruun Theory of Sea-Level Rise as a Cause of Shore Erosion', *The Journal of Geology*, 75(1), pp. 76–92.

SGU (2012) *SGUs Kartvisare: Maringeologi*. Available at: https://apps.sgu.se/kartvisare/kartvisare-maringeologi.html?zoom=402004.25628986035,6132893.565795764,445012.3423060324,6153109.606227845 (Accessed: 16 February 2021).

SGU (2019) *Stranderosion och geologi, Kust*. Available at: https://apps.sgu.se/kartvisare/kartvisare-skanestrand.html?zoom=420120.5066351395,6136499.140047889,441624.54964322556,6147139.161327932 (Accessed: 15 January 2021).

Short, A. D. and Hesp, P. A. (1982) 'Wave, beach and dune interactions in southeastern Australia', *Marine Geology*, 48(3–4), pp. 259–284. doi: 10.1016/0025-3227(82)90100-1.

Sjöfartsverket (2015) *Skärgårdskort*. Available at: https://kartor.eniro.se/?c=55.503944,13.987656&z=11&l=nautical (Accessed: 15 March 2021).

Skoog, M. (2020) Sveriges första strandfodringsprojekt. Ystad Kommun.

Skoog, M. (2021) Personal communication (2021-03-22).

SMHI (2018) *Skydd av stränder i Ystad, fördjupning*. Available at: https://www.smhi.se/klimat/klimatanpassa-samhallet/exempel-pa-klimatanpassning/skydd-av-strander-i-ystad-fordjupning-1.115918 (Accessed: 11 January 2021).

SMHI (2020a) *Framtida medelvattenstånd*. Available at: https://www.smhi.se/klimat/stigande-havsnivaer/framtida-medelvattenstand-1.165493 (Accessed: 25 February 2020).

SMHI (2020b) *Havsnivåhöjning efter 2100*. Available at: https://www.smhi.se/klimat/stigande-havsnivaer/havsnivahojning-efter-2100-1.165465 (Accessed: 25 February 2020).

SMHI (2021) *Klimatindikator - havsvattenstånd*. Available at: https://www.smhi.se/klimat/klimatet-da-och-nu/klimatindikatorer/klimatindikator-havsvattenstand-1.2260 (Accessed: 10 April 2021).

Stive, M. J. F., Nicholls, R. J. and de Vriend, H. J. (1991) 'Sea-level rise and shore nourishment: a discussion', *Coastal Engineering*, 16(1), pp. 147–163. doi: 10.1016/0378-3839(91)90057-N.

Stive, M. J. F. and de Vriend, H. J. (1995) 'Modelling shoreface profile evolution', *Marine Geology*, 126(1–4), pp. 235–248. doi: 10.1016/0025-3227(95)00080-I.

Tegenfeldt, N. and Johansson, O. (2020) *Long-term morphological evolution of Cua Lo inlet, Central Vietnam*. Master Thesis No. 20/5014, Dept. of Water Res. Engrg., Lund University.

TerraMetrics (2021) *Google Maps*. Available at: https://www.google.com/maps/@55.4021998,13.9638246,21135m/data=!3m1!1e3 (Accessed: 15 March 2021).

Thom, B. G. (1984) 'Transgressive and Regressive Stratigraphies of Coastal Sand Barriers in Southeast Australia', *Marine Geology*, 56(1983), pp. 137–158.

Trafikverket (2020) *Ystad hamn och farled, ökad kapacitet och säkerhet - Trafikverket*. Available at: https://www.trafikverket.se/nara-dig/skane/vi-bygger-och-forbattrar/ystadhamnfarled/ (Accessed: 16 February 2021).

Türker, U. and Kabdaşli, M. S. (2004) 'Average sediment dislocation analysis for barred profiles', *Ocean Engineering*, 31(14–15), pp. 1741–1756. doi: 10.1016/j.oceaneng.2004.03.008.

Türker, U. and Kabdaşli, M. S. (2006) 'The effects of sediment characteristics and wave height on shape-parameter for representing equilibrium beach profiles', *Ocean Engineering*, 33(2), pp. 281–291. doi: 10.1016/j.oceaneng.2004.12.016.

U.S. Army Corp of Engineers (1995) 'Design of Beach Fills', *Manual EM 1110-2-3301*, (May), p. 112. Available at: http://www.dtic.mil/dtic/tr/fulltext/u2/a402991.pdf.

US Army Corps of Engineers (1984) *Shore Protection Manual*. U.S. Government Printing Office.

Vellinga, P. (1986) *Beach and dune erosion during storm surges*. Delft: Public Works Department, Delft Hydraulics Laboratory (Report No. 372).

Weisstein, E. W. (no date) *Erf*, *MathWorld - A Wolfram Web Resource*. Available at: https://mathworld.wolfram.com/Erf.html (Accessed: 10 May 2021).

Wolinsky, M. A. and Brad Murray, A. (2009) 'A unifying framework for shoreline migration: 2. Application to wave-dominated coasts', *Journal of Geophysical Research: Earth Surface*, 114(1), pp. 1–13. doi: 10.1029/2007JF000856.

Woodroffe, C. et al. (2012) Approaches to risk assessment on Australian coasts: A model framework for assessing risk and adaptation to climate change on Australian coasts., National Climate Change Adaptation Research Facility. Gold Coast: National Climate Change Adaptation Research Facility (NCCARF Publication 33/12).

Young, A. P. *et al.* (2013) 'Estimating cliff retreat in southern California considering sea level rise using a sand balance approach', *Marine Geology*, 348, pp. 15–26. doi: 10.1016/j.margeo.2013.11.007.

A Appendix

Appendix I – Longshore Diffusivity

Table A.1: Extract from a table developed by Dean (2002), giving the longshore diffusivity from the breaking wave height.

Breaking wave height, H_b [m]	Longshore Diffusivity, ε [m^2/s]
0.3048	0.00199
0.6096	0.0112
1.524	0.111
3.048	0.628
6.096	3.55

Appendix II – Probability Intervals

Table A.2: Estimated probability intervals for the MC simulation.

	1) Sandskogen			2) Hagestad W			3) Hagestad E			4) Sandhammaren		
	min	m.l.	max	min	m.l.	max	min	m.l.	max	min	m.l.	max
d_{50} (mm)	0.227	0.393	0.490	0.246	0.230	0.313	0.243	0.261	0.280	0.228	0.226	0.211
A ($m^{1/3}$)	0.096	0.151	0.156	0.103	0.114	0.125	0.101	0.108	0.114	0.096	0.096	0.090
B (m)	0.5	-	1.5	1	-	1.8	0.7	-	2	1.2	-	1.6
W_B (m)	8.5	-	40	3	-	16	15	-	27	29	-	60
$H_{m0,off}$ (m)	2.19	2.69	3.19	2.64	3.14	3.64	2.40	2.90	3.40	2.27	2.77	3.27
$T_{m,off}$ (s)	9.08	11.08	13.08	8.83	10.83	12.83	8.83	10.83	12.83	8.60	10.60	12.60

Appendix III – Wave Climate

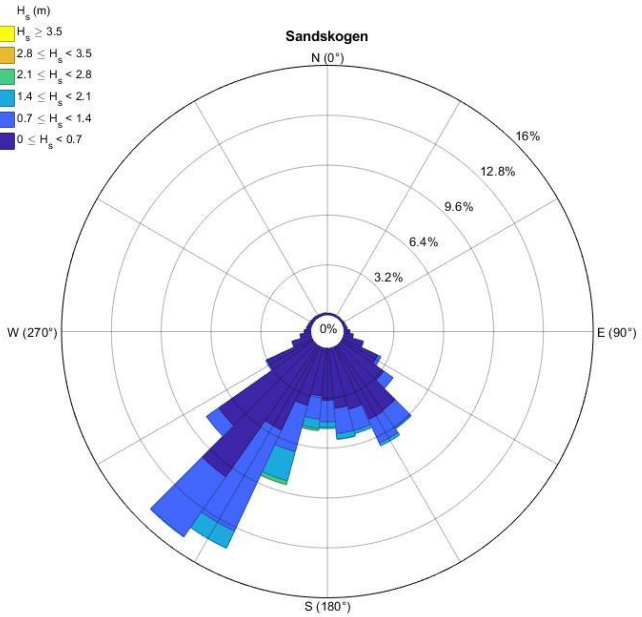

a) Sandskogen

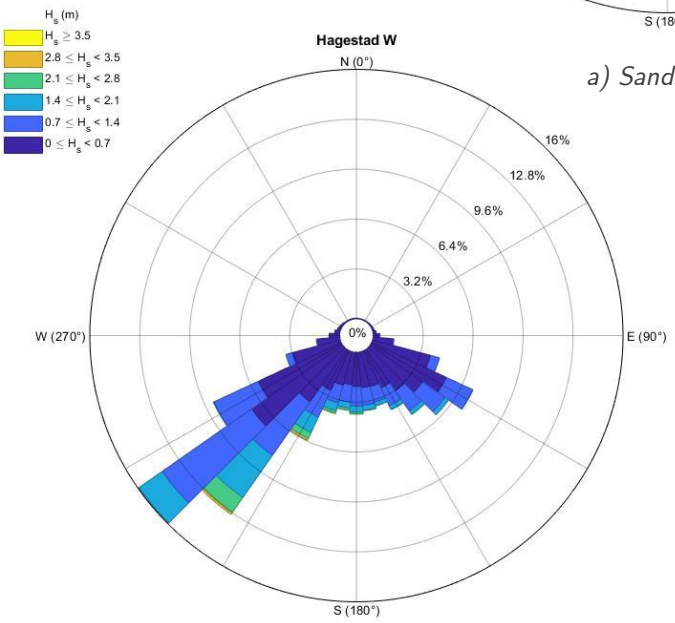

b) Hagestad W

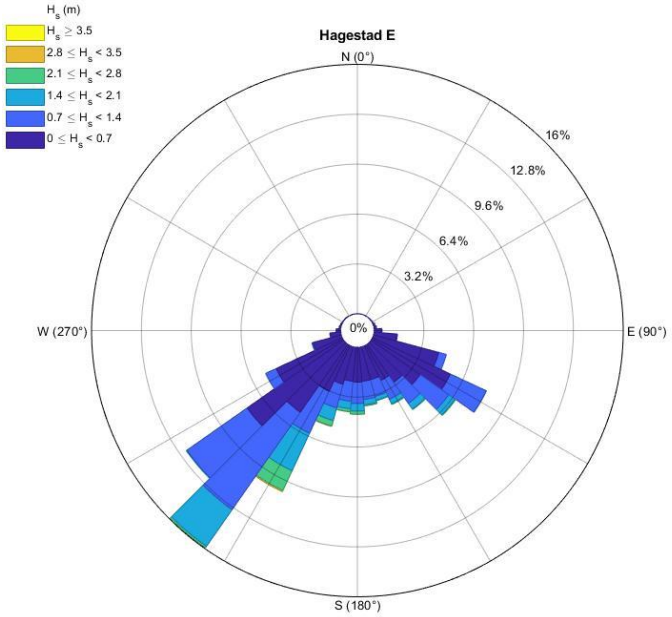

c) Hagestad E

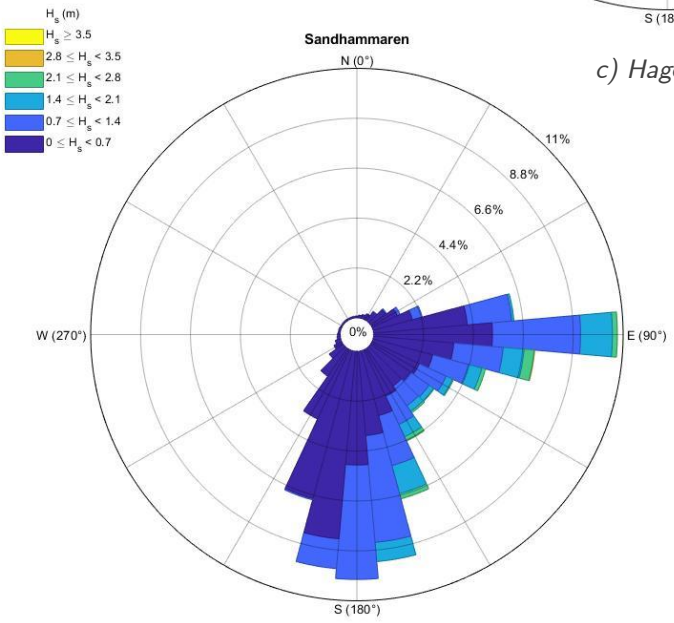

d) Sandhammaren

Figure A.1: Wave roses the transects (year 1979 – 2019). The colours represent the wave height magnitude while the length of the vectors represent the direction frequency.

Appendix IV – Dune Model Usable Sand

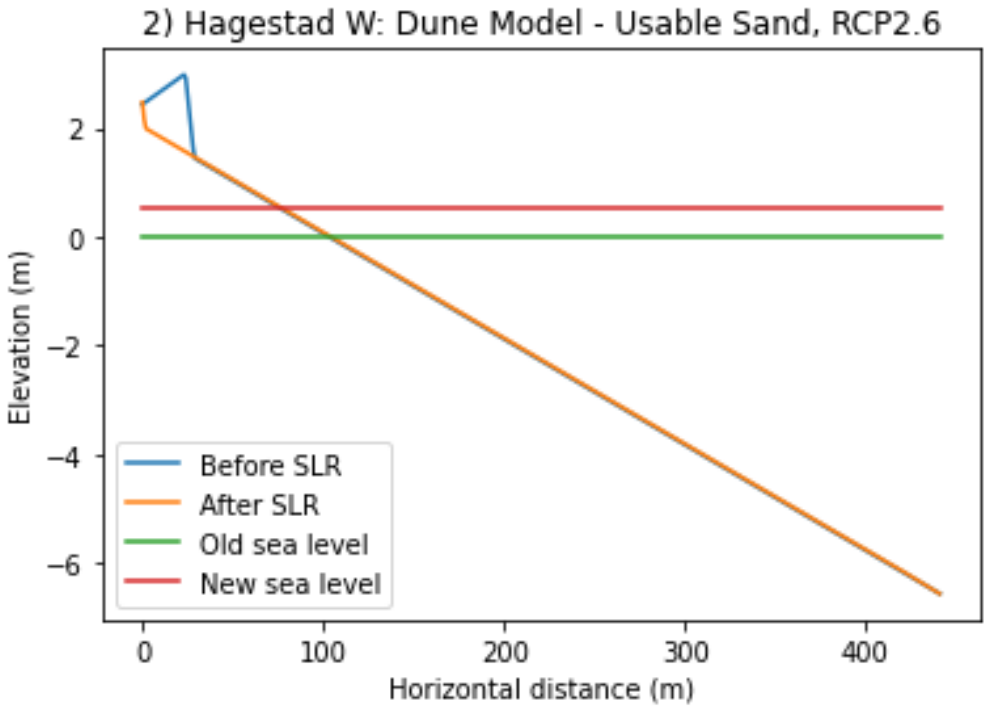

Figure A.2: Schematic figure of the profile of Hagestad W, used in the Dune Model – Usable Sand. The equilibrium profile (beach + subaqueous) is simplified to a straight line. y = 0 corresponds to the mean sea level year 2000.